

Not Gone With the Wind: Long-Run Impact of Herbicidal Warfare in Vietnam*

Gaku Ito[†] Duc Tran[‡] Yuichiro Yoshida[§]

May 10, 2024

Abstract

We investigate the legacies of herbicidal warfare on population size and growth in Vietnam in 2001–2020. The identification strategy exploits the flight-level military records and the plausibly exogenous hamlet-level variation in herbicide exposure around the spray-on, direction-change, and spray-off points of fixed-wing aircraft missions, combined with a fuzzy regression kink design. The elasticity estimate suggests that a 10% increase in herbicide exposure during the Vietnam War is associated with a decrease in population *size* of 1.57–1.93% in 2001 and 2.42–2.8% in 2020. We also find negative associations between herbicide exposure and overall and annual population *growth rates*.

Word Count

7,165 words (excluding the title page and reference)

Keywords

conflict, development, herbicide, historical legacies, Vietnam War

*We are grateful for the insightful and constructive comments from Erik Lin-Greenberg, Masaaki Higashijima, Keisuke Kawata, Yoshiaki Kobayashi, Vally Koubi, Adeline Lo, Wakako Maekawa, Junichi Yamazaki, session participants of the 2022 Annual Meeting of the American Political Science Association, the 2022 Annual Meeting of the Japan Society for International Relations, the 2023 Pacific International Politics Conference, and seminar participants at Hiroshima University, Kyoto University, University of Toyama, and the University of Tokyo. Financial support from the Japan Society for the Promotion of Science (JSPS) is gratefully acknowledged (Grant Numbers 18KT0054 and 20K01464). All remaining errors are ours.

[†]Associate Professor, Graduate School of Economics, Osaka Metropolitan University. 3-3-138 Sugimoto, Sumiyoshi, Osaka 558-8585, Japan. Email: gaku@omu.ac.jp. URL: <https://gaku-ito.github.io>. Corresponding author.

[‡]Research Fellow, Graduate School of Integrated Sciences for Life, Hiroshima University. 1-4-4 Kagamiyama, Higashi-Hiroshima, Hiroshima 739-8528, Japan. Email: tranduc@hiroshima-u.ac.jp. URL: <https://ductran-data.github.io>.

[§]Professor, School of Economics, Kwansei Gakuin University. 1-155 Uegahara Ichiban-cho, Nishinomiya 662-8501, Japan. Email: yuichiro.yoshida@kwansei.ac.jp.

1 Introduction

Does a temporary shock of large-scale violence leave lasting effects on socioeconomic outcomes? In some instances, exposure to large-scale violence persistently depletes human capital and undermines interpersonal and institutional trust (e.g., Grasse, 2023; Lichter, Löffler, and Siegloch, 2020; Nunn and Wantchekon, 2011). Elsewhere, forms of violence foster political engagement, social cohesion, and altruism (e.g., Bauer, Blattman, Chytilová et al., 2016; Berman, Clarke, and Majed, 2023; Blattman, 2009; Gilligan, Pasquale, and Samii, 2014). Several studies also highlight a rapid recovery or catch-up growth of economic and population outcomes in post-war societies, with the impact of wartime destruction remaining short-lived (e.g., Brakman, Garretsen, and Schramm, 2004; Davis and Weinstein, 2002, 2008; Miguel and Roland, 2011; but see Bosker, Brakman, Garretsen et al., 2007).

This article joins the growing literature with new evidence from the herbicide spray in the Vietnam War. While earlier works highlight a powerful recovery from the destruction (Miguel and Roland, 2011), recent literature finds persistent effects of U.S. bombing on development and health outcomes in Cambodia (e.g., Lin, 2022), Laos (e.g., Riaño and Caicedo, 2024; Yamada and Yamada, 2021), and Vietnam (e.g., Palmer, Nguyen, Mitra et al., 2019; Singhal, 2019). Most closely related to this article, Appau, Churchill, Smyth et al. (2021), Le, Pham, and Polacheck (2022), Yamashita and Trinh (2022), and Vuong (2024) examine the legacies of herbicidal warfare. For example, Appau, Churchill, Smyth et al. (2021) underline a persistent negative association between the district-level herbicide exposure and the household agricultural productivity, trust levels, and economic production. In a similar vein, Le, Pham, and Polacheck (2022) find a commune-level positive association between herbicide exposure and the immediate and detrimental prevalence of health disease and mobility disability in the cohort born before the spray mission ended in 1971. Vuong (2024) leverages the difference in dioxin contamination between distinct types of herbicide, Agent Orange and Agent White, for causal identification, which was unknown to high-ranking government officials during the Vietnam War. Vuong (2024) then demonstrates

that the commune-level exposure to dioxin is persistently associated with the present-day disability prevalence, educational attainments, and nightlight intensity.

While the existing insights are valuable, there remain challenges for causal identification primarily due to the commonly used, district-level or commune-level geographic aggregation. This is unfortunate, as the distribution of herbicide dispersal is partly a function of plausibly exogenous, micro-level factors including climate and wind conditions, local geography, and instantaneous decision of aircraft pilots besides initial mission plans and intended targets. The commonly-employed geographic aggregation masks such micro-level variation that would be valuable for causal identification. An alternative, straightforward identification strategy is to exploit the exogenous micro-level variation with geographically less intensive aggregation, which we adopt in this article.

Here, we combine the fine-grained archival data previously unused at the original, *flight*-level scale with a fuzzy regression kink (RK) design to address the identification challenge arising from the nonrandom nature of herbicide exposure. Indeed, historical records suggest that Operation Ranch Hand (1962–1971) missions intended to prevent directly damaging densely populated areas and croplands not under Viet Cong control (MACV, 1969), which would invite bias into naive comparisons. To surmount the identification challenge, our RK strategy leverages the *uncontrollable*, natural experimental variation in the hamlet-level exposure to herbicide around the spray-on, direction-change, and spray-off points of fixed-wing aircraft missions. To capture the micro-level variation in herbicide missions, we rely on the flight-level records documented in the Stellman-National Academy of Sciences version of the Herbicide Report System file (S-NAS HERBS, Stellman, Stellman, Christian et al., 2003; Stellman, Stellman, Weber et al., 2003).

The RK analysis reveals lasting legacies of herbicidal warfare. The elasticity estimate suggests that a 10% increase in herbicide exposure, which is observed within a 1 km distance from the spray start, turn, and end points, is associated with a 2.42–2.8% decrease in population size in 2020. The analysis also reveals negative associations between the herbicide

shock and population *growth rate* in 2001–2020. While the discrepancy might arise from different units of analysis, the previously unseen patterns run counter to the conventional wisdom of a powerful recovery of population from wartime destruction.

2 Data

2.1 Stellman-National Academy of Sciences HERBS File

To measure the landscape of herbicide spray, we rely on the military archival records of the Stellman-National Academy of Sciences version of the Herbicide Report System file (S-NAS HERBS) database (Stellman, Stellman, Christian et al., 2003; Stellman, Stellman, Weber et al., 2003).¹ The S-NAS HERBS is a compilation of military mission records of the HERBS file originally developed by the U.S. Department of Defense with corrections, containing 9,141 reports of the spray missions with several spray methods (i.e., fixed-wing aircraft, helicopters, and ground-spraying) in 1961–1971. A record in the database corresponds to a single mission with one or more spray paths. Figure 1 shows the geographical and temporal distributions of the mission records. As elaborated in detail below, the following analysis relies on the aircraft missions that dispersed approximately 95% of herbicides (Stellman, Stellman, Christian et al., 2003, 681–682).²

A noteworthy aspect of the S-NAS HERBS is its geocoding accuracy. Besides mission dates, spray methods, agent, and gallonage information, the database documents “the actual flight paths taken by Ranch Hand aircraft as they carried out their spray missions,” with the “locations at which the aircraft switched directions or turned off and on their spray nozzles” (Stellman, Stellman, Weber et al., 2003, 323), thereby providing a detailed landscape of spray missions.³

¹We web-scraped the mission records from the Agent Orange Warehouse website. Available at: <http://www.workerveteranhealth.org/milherbs/new/>, accessed August 29, 2021. See Appendix A for details.

²We discard 91 errant entries of “fixed-wing aircraft” records with single (not multiple) geocoordinates.

³To navigate aircraft and record spray-on, direction-change, and spray-off points, the tactical air navigation (TACAN) system distance measuring equipment (DME) was well-developed in Southeast Asia by the

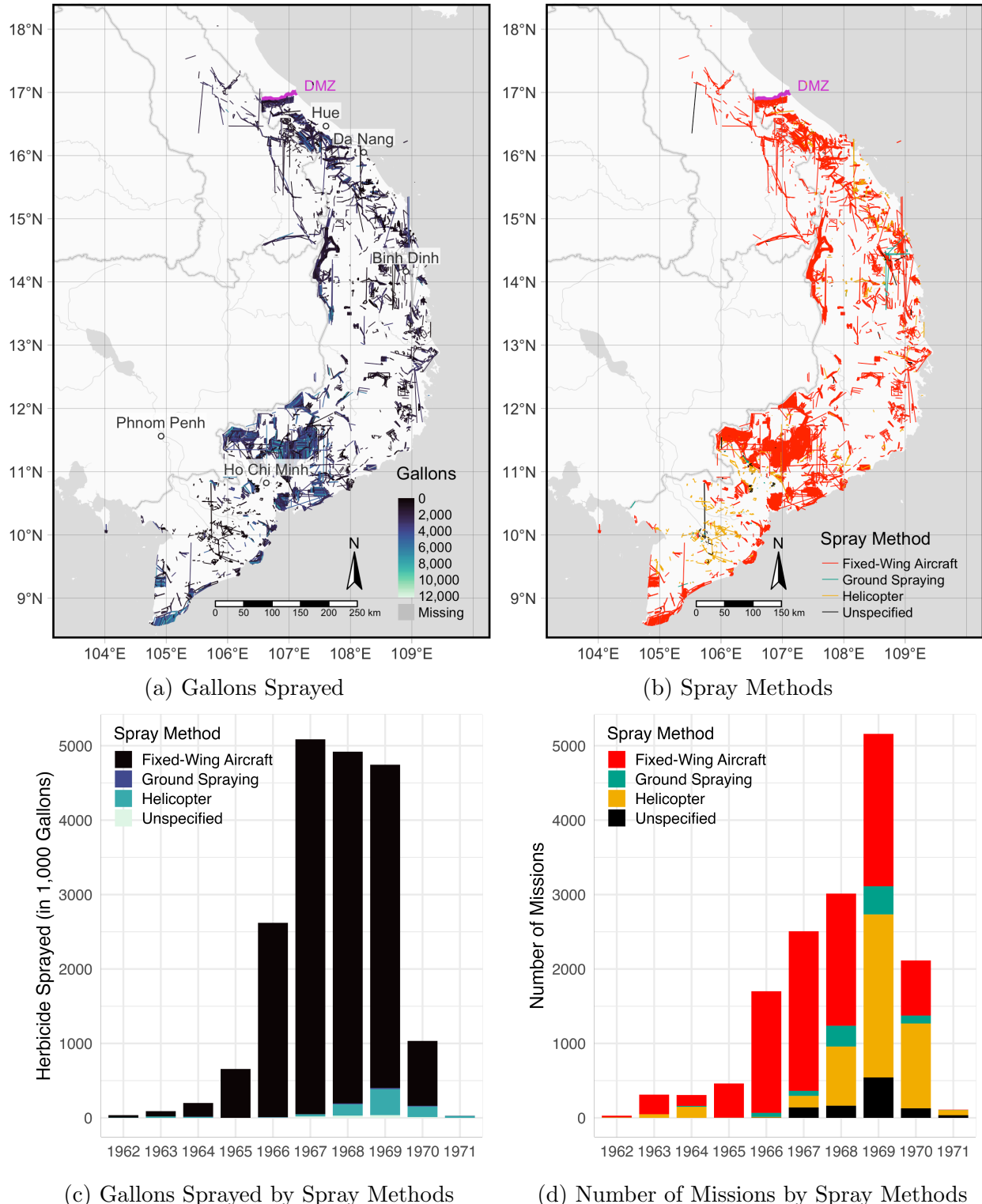


Figure 1: Herbicide Spray Missions

Notes: Segments in maps represent the spray paths. (a) Shading is proportional to the quantity of sprayed herbicide in gallons sprayed by individual spray legs (straight lines without a turn). (b) Colors indicate distinct spray methods. Thick gray lines indicate international borders. Thin gray lines and polygons represent major water bodies. (c), (d) Yearly distribution of herbicide spray (in 1,000 gallons) and spray methods, omitting four helicopter missions in 1961.

2.2 Treatment: Herbicide Exposure

We use hamlets in South Vietnam as the unit of analysis in the following analysis, based on the geocoordinates (points) recorded in the Vietnam Hamlet Evaluation System (HES) Gazetteer Data (Douglass, 2011). To quantify the hamlet-level exposure to herbicide, we broadly follow the distance-weighted approach of Stellman and Stellman (1986, 309) as:

$$\text{HERB}_i = \sum_{j \in \mathcal{H}} G_j \cdot e^{-\lambda D_{ij}}, \quad (1)$$

where i indexes hamlets and j spray flight “legs” of the fixed-wing aircraft missions. Following Stellman, Stellman, Weber et al. (2003, 325), we first split individual flight paths (contiguous lines) into distinct flight legs indicated by the straight lines without turns. As the gallonage information is aggregated at the mission level, we divide and assign the total mission-level herbicide quantities to individual legs in proportion to its spray run length.⁴ G_j indicates the quantity of the herbicides sprayed in leg j in gallons, \mathcal{H} is a set of all spray flight legs, and D_{ij} represents the geodesic distance between hamlet i and flight leg j . $\lambda = \frac{\ln(2)}{D^{\text{Half}}}$ is an arbitrary parameter, where D^{Half} determines the geodesic distance at which the herbicide exposure decays to the half of a “direct” (zero-distance) hit with $D_{ij} = 0$, with the baseline of $D^{\text{Half}} = 500$ meters (i.e., $e^{-(\ln(2)/500) \times 500} = 0.5$). For a robustness check purpose, Appendix C.2 reestimates the main regressions with alternative half-decay distance parameters of 100 meters, 250 meters, and 1 km.

2.3 Outcome: Population Size and Growth Rate

The following analysis focuses on contemporary population size and population growth rate as outcome variables. We rely on the WorldPop data, which provides geographically disaggre-

1960s. During mission flights, TACAN/DME continuously offered geographical navigation using the (short) ultra high frequency (UHF) radio range (Rowley, 1975). An essentially same navigation system guided civic aviation until the mid-1990s or before the civic use of the global positioning system (GPS).

⁴For example, if a mission includes one flight with four legs (three turns) with an equal leg length sprayed 1,000 gallons in total, we assign 250 gallons to each flight leg.

gated records of population estimates at 100 meter level on an annual basis in the 2001–2020 period.⁵ To construct the population size variable, we first extract the annual records of population counts at the hamlet locations, and take the natural logarithm of the variable after adding 1. The (logged) overall and annual population growth rates, respectively, are measured as $\ln \text{Population}_{2020} - \ln \text{Population}_{2001}$ and $\ln \text{Population}_t - \ln \text{Population}_{t-1}$.

2.4 Covariate: Key Spray Targets and Related Attributes

To facilitate the empirical analysis, we combine archival sources and several geographical databases to construct three sets of covariates. The first set of covariates measures the proximity to the key spray targets. Operation Ranch Hand involved two primary objectives, forest defoliation and destruction of enemy food supplies, with key targets including “base camps and fire support bases...lines of communication, enemy infiltration routes, and enemy base camps” (Institute of Medicine, 1995, 85). The mission authorization process also intended to prevent damage to densely populated areas and crops not under Viet Cong (VC) control (MACV, 1969). To measure proximity to the key spray targets, we include the prevalence of VC control in 1967–1969 (HES, McCormick, 2021), geodesic distances to suspected areas of North Vietnam Army (NVA) bases (Enemy Base Area File, BASFA), U.S. Air Force and Navy bases, U.S. Army and Marine troops in 1961–1971 (S-NAS-HERBS), and roads (including trails, *Indochina Atlas*), average hamlet population size in 1967–1969 (HES, Douglass, 2011), and dummy variables for the presence of rice croplands and slash and burn cultivation (*Indochina Atlas*), with the details described in Appendix A.4.⁶

Second, geographic covariates include mean elevation and its standard deviation as a proxy of terrain ruggedness (USGS, 1996), soil suitability for rice cultivation (Zabel, Putzenlechner, and Mauser, 2014), distance to rivers, flow accumulation (Lehner, Verdin, and Jarvis,

⁵ Available at: <https://www.worldpop.org>, accessed August 6, 2021. Due to errant entries, we exclude the population estimates in 2000 from the analysis.

⁶ Where multiple hamlet-month observations are available, VC control measures the average of a dummy variable indicating VC control. To measure road proximity and cropland presence, we georeferenced and image-processed the maps of *Indochina Atlas* compiled by the Central Intelligence Agency (CIA) in 1970. For the locations of NVA bases, we rely on the Enemy Base Area File (BASFA), July 1, 1967–July 1, 1971.

2008), a dummy variable for forest presence (*Indochina Atlas*), and average precipitation and wind speed (1970–2000, Fick and Hijmans, 2017). Finally, historical covariates are the number of hamlets within a 30 km radius, distance to railways (*Indochina Atlas*) and international borders (as of the Vietnam War period), and the average of the annual minimum distance to aerial bombing drop points in 1965–1971 (Defense Digital Service, 2016).⁷

3 Identification Strategy: Fuzzy Regression Kink

To explore the evidence of causal effects, we rely on a fuzzy regression kink (RK) design that exploits the exogenous fluctuations in herbicide exposure within geographically small areas around the spray start, turn, and end points. Recall that the S-NAS-HERBS database that documents the “actual flight paths” and the “locations at which the aircraft switched directions or turned off and on their spray nozzles” (Stellman, Stellman, Weber et al., 2003, 323).⁸ The core idea behind our RK strategy is that the *exact* locations at which aircraft makes turns and turned on and off spray nozzles and the herbicide dispersal were, at least partly, *uncontrollable*. Besides intended targets, the *realized* distribution of herbicide was driven by plausibly exogenous micro-level factors including climate conditions, wind, terrain, and turbulence from the aircraft as well as ground fire hits (Institute of Medicine, 1995, 86–87). Consistent with the identification idea, “[t]he responsibility for flying the C-123 during the crucial spraying part of each mission was shared between the pilot and the copilot,” with the pilot having “control of the switches which started and stopped the spray” (Buckingham, 1982, 37). As such, instantaneous decision of aircraft pilots and drift due to the disturbing factors jointly determined the spray dispersal, which inevitably deviated from the initial mission plans and generated haphazard, natural-experimental variation in

⁷The 30 km cutoff reflects the historical facts of Ranch Hand missions and standard error clustering in the regression estimation. See model specification section for details.

⁸See footnote 3 for the aircraft navigation system in the Vietnam War period. Also note that a fuzzy RK design allows incomplete manipulation while addressing measurement errors in the treatment and the running variable (Card, Lee, Pei et al., 2015, 2467–2469). Appendix B investigates potential nonlinearity in the covariate distributions across the kink point, and Appendix C examines model dependence and how model specification influences the main findings.

the herbicide distribution.⁹

Consequently, within geographically small areas around the spray start, turn, and end points, the realized herbicide dispersal generates a discontinuous *slope change*, or a discontinuity in the first derivative, in the distribution of herbicide exposure, which remains uncorrelated with potential confounding forces. Our RK strategy leverages this natural experimental kink in the treatment function to derive causal identification. Intuitively, we compare hamlets that were barely covered by spray flights and received direct hits (i.e., “treated” hamlets with greater herbicide exposure due to direct hits) with hamlets that were sufficiently close to but located barely outside of the spray flight paths and received indirect hits (i.e., “control” hamlets with less exposure due to accidental drifts). Located within geographically small areas, these treated and control hamlets should have similar (or more precisely, no kink in) geographic, historical, and socioeconomic attributes prior to herbicide exposure, which we empirically validate in the following section.¹⁰

Here, we adopt a RK design rather than a regression discontinuity (RD) design given the probable drifts of herbicide outside the areas with direct hits. We rely on a fuzzy, not sharp, RK design given the unknown slope change parameter of the herbicide exposure (treatment) function at the kink point as well as probable measurement errors in the treatment and the running variable retrieved from the archival military records (Card, Lee, Pei et al., 2015, 2464–2467).

3.1 Running Variable

The RK design requires a subset of sample hamlets located within sufficiently small geographic areas around the spray start, turn, and end points. The analysis also requires the corresponding distance measure between hamlet locations and the spray start, turn, and end

⁹To illustrate, approximately 29% of aircraft sorties were intercepted by ground fire in 1966 (Institute of Medicine, 1995, 86), and the crop damage induced by drift on defoliation missions was greater than the damage by crop destruction missions (National Academy of Sciences, 1974, S-5).

¹⁰As discussed below, a valid RK design requires that covariate distributions evolve smoothly across the kink point as well as the smoothness of the running variable distribution.

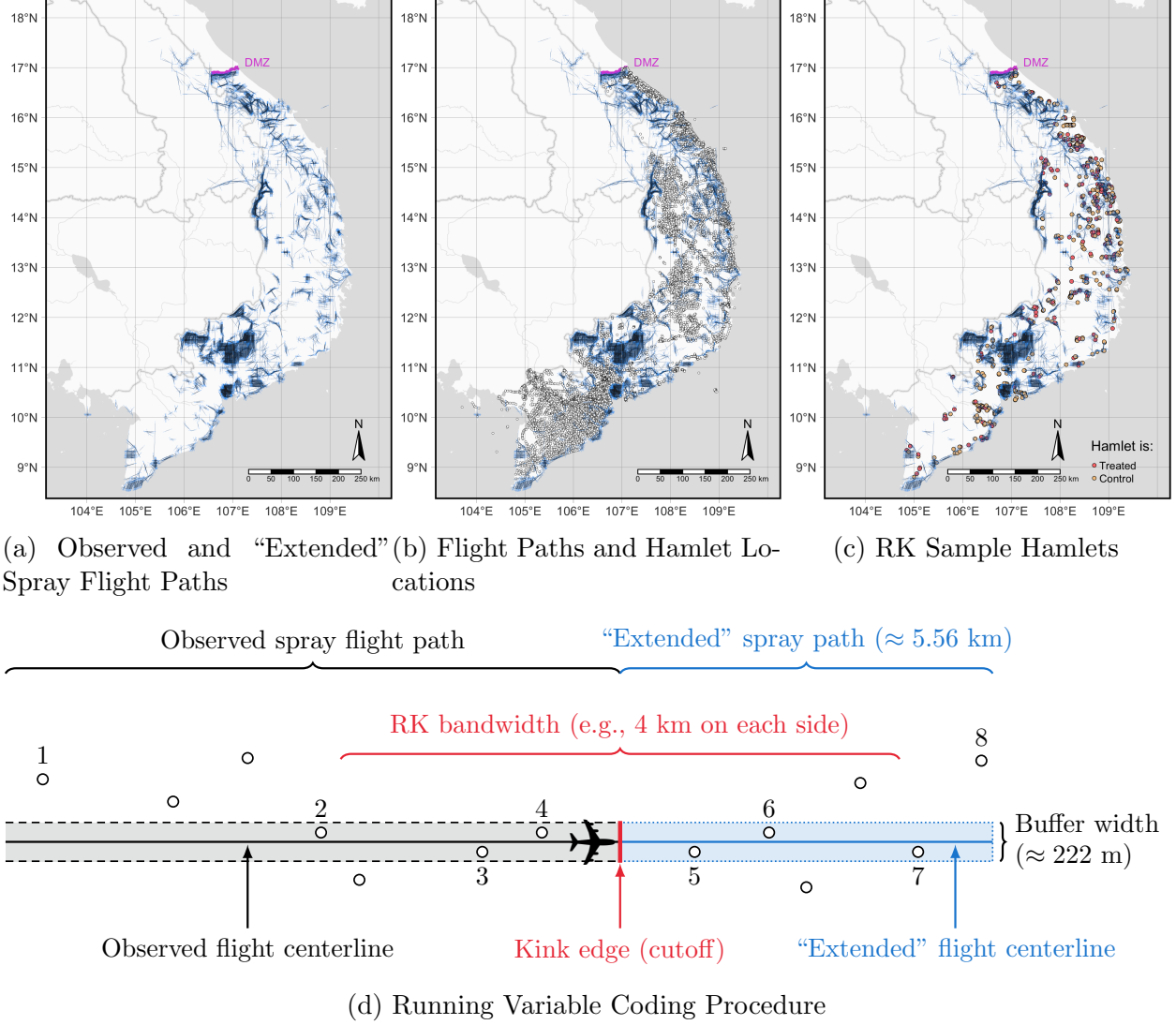


Figure 2: Spray Flight Paths, Hamlet Locations, and the RK Running Variable Coding Procedure
Notes: (a) Black polygons represent observed flight paths, and blue polygons indicate the extended flight paths with a 0.05 degree (≈ 5.56 km) distance from the start/turn/end points with a 111 meter buffer on each side (222 meters in total). Of the 14,733 hamlets (Panel (b)), hamlets covered by observed flight polygons with a 222 meter buffer are categorized into the treatment groups (red dots), while the hamlets only covered by a blue polygon are categorized into the control group (yellow dots; Panel (c)). (d) Vertical thick segment indicates a kink edge. Dots and horizontal solid segments, respectively, represent hamlet locations and observed and “extended” spray flight paths. Dashed (dotted) segments and shades represent the buffer around the observed (extended) spray path.

points as the running variable as well as a dummy variable indicating actual spray hits.

The coding procedure involves several steps. First, we extend the recorded flight paths of fixed-wing aircraft missions from the flight start, turn, and end points by an arbitrary length of 0.05 degree ≈ 5.56 km. Second, we add buffers of 0.001 degree ≈ 111 meter width to both

sides (222 meters) of the extended flight paths, as graphically illustrated by Figure 2(a). The baseline extension length of 5.56 km and the 222 meter buffer width mimic ordinary spray flights in Operation Ranch Hand. A routine fixed-wing aircraft mission involved multiple aircraft and dispersed herbicide at the airspeed of 130–150 knots (240–278 km/h) and an altitude of 150 feet, with each aircraft covering a (laterally contiguous) swath of 80 meter wide and 16 km long (Buckingham, 1982, 37, 132; Institute of Medicine, 1995, 25, 86–87; Stellman, Stellman, Weber et al., 2003, 327). An extension length of 5.56 km approximately corresponds to the “less-than-one-half-minute-away” distance from the observed kink point at the airspeed of 240–278 km/h ($= 4\text{--}4.63 \text{ km/m}$). A 222 meter buffer width similarly approximates the combined swath of a routine spray mission involving three airplanes. This 222 meter or three-aircraft approximation also reflects the historical fact that three C-123 Provider airplanes were assigned to Operation Ranch Hand until 1964, and the number of C-123s increased to 12 in 1965 and then to 36 in 1967 (Institute of Medicine, 1995, 86).

Third, we overlay the extended flight path polygons onto hamlet locations. The hamlets covered by the flight path polygons without the 5.56 km extension are coded as “treated,” while those only covered by the extended parts are categorized into the control group (Figures 2(b) and (c)). For example, in Figure 2(d), among the hamlets located within the 5.56 km distance from the kink edge, polygon edges corresponding to the spray start, turn, end points, hamlets 2–4 are categorized into the treatment group while hamlets 5–8 are categorized into the control group. We then measure the geodesic distance between hamlet locations and the nearest kink edges to assign running variable to individual hamlets.¹¹

As in Figure 2(c), the full RK sample includes the hamlets that are geographically covered by the observed or extended flight path polygons with the kink edge distance smaller than 5.56 km extension length. The geoprocessing leaves us a sample of 716 hamlets (4.86% of 14,733 hamlets in panel (b)) in 125 districts (38 provinces) in South Vietnam.

¹¹The illustration here assumes that single spray flights cover single hamlets. When more than one spray flight covers single hamlets, we modify the coding rule for the treated hamlets not to categorize the hamlets located close to one kink edge (e.g., 100 meters) but far from another edges (e.g., 10 km $>$ 5.56 km threshold) into the treatment group. See Appendix A.3 for details.

3.2 Model Specification

Our RK estimation builds upon the following two-stage model:

$$\ln \text{HERB}_{hd} = \gamma \text{EdgeDist}_{hd} + \delta \text{EdgeDist}_{hd} \times \mathbb{1}[\text{EdgeDist}_{hd} \geq 0] + \zeta \mathbb{1}[\text{EdgeDist}_{hd} \geq 0] \\ + \mathbf{X}_{hd}^\top \boldsymbol{\beta} + \eta_d^{\text{District}} + \kappa_{a[h]}^{\text{Agent}} + \theta_{k[h]}^{\text{End-edge}} + \iota_{k[h]}^{\text{Pre-1967}} + f_1(\text{Lon}_{hd}, \text{Lat}_{hd}) + e_{hd}, \quad (2)$$

$$Y_{hd} = \tau \ln \widehat{\text{HERB}}_{hd} + \lambda \text{EdgeDist}_{hd} + \nu \mathbb{1}[\text{EdgeDist}_{hd} \geq 0] + \mathbf{X}_{hd}^\top \boldsymbol{\xi} + \pi_d^{\text{District}} + \rho_{a[h]}^{\text{Agent}} \\ + \phi_{k[h]}^{\text{End-edge}} + \psi_{k[h]}^{\text{Pre-1967}} + f_2(\text{Lon}_{hd}, \text{Lat}_{hd}) + u_{hd}, \text{ if } |\text{EdgeDist}_{hd}| \leq b \quad (3)$$

where h , d , a , and k , respectively, index hamlets, districts, herbicide agents, and kink edges. HERB denotes the herbicide exposure score, EdgeDist is the geodesic distance from the kink edges in kilometers recentered at zero, and $\mathbb{1}[\text{EdgeDist} \geq 0]$ is a dummy variable which takes one if $\text{EdgeDist} \geq 0$ (treatment group) and zero otherwise (control group).¹² \mathbf{X} is a vector of hamlet-level covariates, and $f_1(\text{Lon}, \text{Lat})$ and $f_2(\text{Lon}, \text{Lat})$ are two-dimensional cubic polynomials of hamlet geocoordinates to screen out spatial trends.¹³ η^{District} and π^{District} are (South Vietnam) district fixed effects, and κ and ρ are herbicide agent fixed effects.¹⁴ $\theta^{\text{End-edge}}$ and $\phi^{\text{End-edge}}$ are end-edge fixed effects which take one if a hamlet's running variable is distance to a spray flight end edge and zero otherwise (i.e., a flight start or turn edge); and $\iota^{\text{Pre-1967}}$ and $\psi^{\text{Pre-1967}}$ are fixed effects indicating a hamlet's running variable measured as the distance to the flight leg edges of pre-1967 missions, before the increase of the number of aircraft from 12 to 36 assigned to Operation Ranch Hand mentioned above. The panel setup replaces the second-stage outcome with annual population growth rate and adds a year fixed

¹²The specification includes $\mathbb{1}[\text{EdgeDist}_{hd} \geq 0]$ and thereby allows discontinuity in the treatment function at the kink point. When the kernel is symmetric (e.g., a uniform kernel), the asymptotic bias and variance of the RK estimand are not affected by the continuity imposition (Card, Lee, Pei et al., 2012, 2015).

¹³Linear, quadratic, and fifth-order polynomials of longitude and latitude yield qualitatively similar results.

¹⁴The herbicide agent fixed effect has five categories: “Blue,” “Orange,” “Purple,” “White,” and “Others.” Given the small numbers of observations, we put “Pink” and “Unknown” into “Others” category.

effect to the right hand side of the regression models.¹⁵ Following Card, Lee, Pei et al. (2012, 2015, 2017), our RK estimation relies on an uniform (rather than triangular) kernel, and the baseline setup uses a bandwidth of $b = 4$ kilometers (522 hamlet observations). Intuitively, a 4 km bandwidth approximates the “one-minute away” distance at the typical airspeed of 4–4.63 km/m (= 240–278 km/h) of fixed-wing aircraft missions. To ensure that the fixed bandwidth choice does not drive the results, we replicate the RK estimates with alternative bandwidth sizes.

The parameter of interest is τ in the second-stage (equation 3), which substantively captures the average effect of a marginal increase in ln HERB on the outcome at the cutoff. Formally, τ can be interpreted as the treatment-on-the-treated (TT) effect (Florens, Heckman, Meghir et al., 2008) or the local average response (LAR) of herbicide exposure (Altonji and Matzkin, 2005), instrumented by EdgeDist $\times \mathbb{1}[\text{EdgeDist} \geq 0]$ in the first stage (Card, Lee, Pei et al., 2015).¹⁶

Several aspects of the specification are worth explanations. Given the asymptotic results of Pei, Lee, Card et al. (2022), we adopt a local linear specification given the relatively small sample size. We also rely on district, agent, end-edge, and pre-1967 mission fixed effects instead of the ideal flight or leg fixed effects due to limited sample size. Nonetheless, the specification reflects the historical fact that South Vietnam Government both at the national and local levels and the U.S. jointly controlled the herbicide missions (Buckingham, 1982, 36–38; Institute of Medicine, 1995, 86).¹⁷ District fixed effects subsume the regional variation in

¹⁵With abuse of notations, the panel version of the second-stage model is:

$$Y_{hdt} = \tau \ln \widehat{\text{HERB}}_{hd} + \lambda \text{EdgeDist}_{hd} + \nu \mathbb{1}[\text{EdgeDist}_{hd} \geq 0] + \mathbf{X}_{hd}^\top \boldsymbol{\xi} + \pi_d^{\text{District}} + \rho_{a[h]}^{\text{Agent}} \\ + \phi_{k[h]}^{\text{End-edge}} + \psi_{k[h]}^{\text{Pre-1967}} + \eta_t + f_2(\text{Lon}_{hd}, \text{Lat}_{hd}) + e_{hdt},$$

where η_t represents year fixed effect, with the corresponding first-stage model specified analogously.

¹⁶Seen from the instrumental variable (IV) perspective, a key identification assumption is that the instrument affects the outcome (slope change) only through the treatment (slope change). Violation of this exclusion restriction condition invalidates the smoothness assumption for a valid RK design (Card, Lee, Pei et al., 2015). We briefly validate the identification assumptions below while relegating the details to Appendix B.

¹⁷The authorization process also involved the U.S. Ambassador, the U.S. Military Assistance Command, and the Corps Tactical Zones (CTZs). Dell and Querubin (2018) use the CTZ (Corps I-II) boundary as one

the authorization process and other district-level differences of counterinsurgency strategies; and the remaining fixed effects absorb the types of chemical shocks (agent fixed effects), aircraft directions (end-edge fixed effects), and overall intensity of herbicide missions and potential military significance of nearby targets (pre-1967 fixed effects; Figures 1(c), (d)).

Throughout the analysis, we rely on the two-stage least-squares (2SLS) estimator. To account for the increased error due to the two-stage estimation and potential error dependence across space, we report Conley's (1999) standard errors robust to spatial clustering with a 30 km cutoff.¹⁸ Appendix A reports descriptive statistics of the variables.

3.3 Identification Assumption

A valid fuzzy RK design hinges on the smoothness assumption, which yields two testable implications: First, the density of the running variable is sufficiently smooth, or continuously differentiable at the cutoff; and second, predetermined covariates evolve smoothly around the kink point (Card, Lee, Pei et al., 2012, 2015, 2017).

Following literature (Bana, Bedard, and Rossin-Slater, 2020; Card, Johnston, Leung et al., 2015; Card, Lee, Pei et al., 2015; Landais, 2015), we validate the smoothness assumption with the running variable and covariate distributions in three ways. First, Figure B.1 in the Appendix examines the continuity of the running variable distribution using the polynomial estimator of Cattaneo, Jansson, and Ma (2020), and fails to detect statistically significant discontinuity at the kink point ($t = -0.209$ and $p = 0.835$). Second, we test for the kink in the running variable distribution using polynomial regressions.¹⁹ As reported in

of the sources for causal identification. As the CTZ boundaries follow the province boundaries, district fixed effects subsume the difference in counterinsurgency strategy across CTZs and local governments.

¹⁸We use a 30 km cutoff to reflect the combat range of aircraft missions in which a C-123 airplane covered a swath of 80 m wide and 16 km long (Buckingham, 1982, 132). A 30 km cutoff approximately reflects the 16-km range as a radius. The sample mean (median) of the aircraft spray legs is 18 km (16.48 km).

¹⁹Formally, and with abuse of notation, we first aggregate the hamlet observations using bins with different sizes based on the running variable and then estimate the following regression model:

$$N_b^{\text{obs.}} = \beta \mathbb{1}[\overline{\text{EdgeDist}}_b \geq 0] + \sum_{p=1}^P \left[\gamma_p \overline{\text{EdgeDist}}_b^p + \delta_p \overline{\text{EdgeDist}}_b^p \cdot \mathbb{1}[\overline{\text{EdgeDist}}_b \geq 0] \right] + e_b,$$

Figure B.2 in the Appendix, the polynomial regressions fail to detect a slope change in the running variable distribution around the kink point.

Finally, Figure B.3 in the Appendix presents a series of placebo kink estimates with the covariates, *including* hamlet population in 1967–1969 (during Operation Ranch Hand), as the left-hand-side variable using a reduced-form version of our RK specification. Again, and consistent with the smoothness assumption, most of the placebo regressions does not reveal a discernible slope change at the kink point. Exceptions are the substantively small but statistically significant slope change in wind speed and the distance to U.S. bases plausibly arising from random chance or sampling error. Indeed, as reported in Appendix B.2, the same randomization inference exercise introduced in the next section fails to negate that the covariate kink arises by chance. Moreover, Appendix C.1 finds little evidence of model dependence, suggesting the minor role of the marginally significant covariate kink in influencing our RK estimates.

4 Results

Figure 3 displays the distributions of herbicide exposure (first-stage association; panel (a)) and population size in 2020 (reduced-form association; panel (b)), given hamlet geocoordinates and fixed effects.²⁰ As the fuzzy RK estimand can be written as the ratio of the reduced-form and first-stage associations, the co-evolving slope change provides a graphical

where b indexes bins, $N^{\text{obs.}}$ reflects the number of observations in each bin, $\overline{\text{EdgeDist}}$ is the midpoint of EdgeDist of each bin, and P is the polynomial order. δ_1 captures the slope change of the probability density function of the running variable at the kink point. Not to violate the smoothness assumption, δ_1 should remain indistinguishable from zero.

²⁰The RK estimand, τ_{RK} , can be written as the ratio of the reduced-form slope change (i.e., slope change in the outcome function) relative to the first-stage slope change (i.e., slope change in the treatment function) at the kink point as (Card, Lee, Pei et al., 2012, 2015):

$$\tau_{\text{RK}} = \frac{\frac{\lim_{v_0 \downarrow 0} d(\mathbb{E}[Y|V=v])}{dv} \Big|_{v=v_0} - \frac{\lim_{v_0 \uparrow 0} d(\mathbb{E}[Y|V=v])}{dv} \Big|_{v=v_0}}{\frac{\lim_{v_0 \downarrow 0} d(\mathbb{E}[D|V=v])}{dv} \Big|_{v=v_0} - \frac{\lim_{v_0 \uparrow 0} d(\mathbb{E}[D|V=v])}{dv} \Big|_{v=v_0}},$$

where V denotes the running variable, v_0 the kink point, and D the treatment.

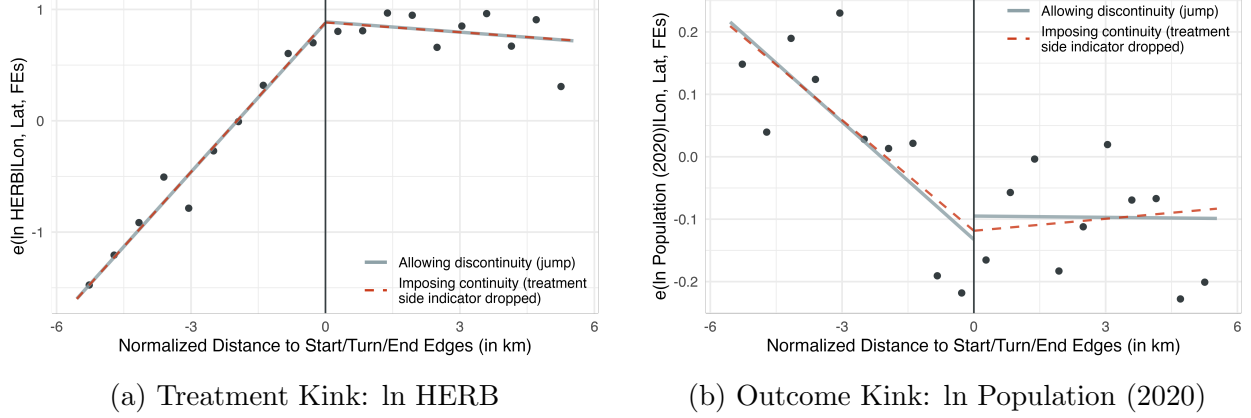


Figure 3: Discontinuous Slope Change in the Treatment and Outcome Functions at the Kink Point
Notes: Dots represent the binned frequencies, and solid and dashed lines show linear regression fits adjusting for longitude, latitude, and agent and district fixed effects. Solid line allows discontinuity (as equation 2), while the dashed line imposes continuity at the kink point by dropping the treatment-side dummy variable. The bin size is selected by the integrated mean squared error (MSE)-optimal mimicking variance evenly-spaced method using spacing estimators (Calonico, Cattaneo, and Titiunik, 2015).

but initial empirical evidence of herbicide legacies on contemporary population outcomes. In the following, we first report the cross-sectional RK estimates with population size as the outcome. We then extend the analysis with alternative growth rate and panel specifications across different bandwidth sizes, followed by a brief summary of robustness checks.

4.1 Population Size Estimates

Table 1 reports the RK estimation results with population size in 2001 (Panel A) and 2020 (Panel B) as the outcome, along with the first-stage estimates. Model (1) is the baseline model without additional controls besides the two-dimensional polynomial of longitude and latitude and fixed effects. Models (2) to (4) consecutively add the proximity to the key targets, geographical characteristics, and historical attributes as covariates. To address potential spillover effects, Model (5) adjusts for the spatially-lagged treatment with the 30 km neighbor cutoff in addition to the full set of covariates in model (4). Note that given the limitation in data availability and the historical facts, some of the covariates can partly be posttreatment (e.g., bombing point distance, 1965–1971). The models with covariate adjustments, therefore, do not necessarily provide conservative estimates due to possible

posttreatment bias of unknown directions and should be interpreted with caution.

Table 1 confirms the graphical evidence of Figure 3 and underlines the herbicide legacies. Across model specifications, the first-stage, treatment kink estimates are substantively and statistically significant (Panel A). The second-stage coefficients on $\ln \text{HERB}$ are also consistently signed negative and retain the statistical significance at the conventional 5% level (Panels B and C). Note also that uninstrumented ordinary least squares (OLS) estimates reported in Appendix Table A.2 substantively underestimate or even fail to reveal the negative association, suggesting that nonrandom herbicide assignment invites bias into naive comparisons. Moreover, the coefficient stability suggests that the estimates are unlikely to be driven by an arbitrary covariate adjustment choices, which is of a particular concern in RK applications (Ando, 2017) and we further investigate in Appendix C.1. The negative association also remains visible across the outcomes, population size in 2001 and 2020.

As an initial robustness check, Table 1 also reports three randomization inference results.²¹ First, an important concern for RK applications is the misspecification of the underlying nonlinearity such that one falsely specifies a quadratic relationship or curvature with no kink as a discontinuous slope change (Ganong and Jäger, 2018). To guard against the misspecification bias, Table 1 reports kink point (KP) randomization p -value obtained from the reduced-form permutation test (Ganong and Jäger, 2018).²² For the exercise, we first generate 10,000 placebo kink points randomly drawn from a uniform distribution, $\mathcal{U}(-4 \text{ km}, 4 \text{ km})$. We then consecutively estimate the reduced-form version of the RK model with the subsample within baseline 4 km bandwidth around each placebo kink point to obtain the empirical distribution of placebo estimates. The two-sided p -value is computed by doubling the minimum of the fraction of placebo estimates no smaller than or no greater than the actual reduced-form coefficient. Second, another intuitive approach of random-

²¹Randomization exercise relies on the reduced-form and first-stage models as randomization inference cannot be applied without additional assumptions to unobservable subgroups such as compilers.

²²If our RK specification correctly captures a discontinuous slope change, we would be unlikely to see a slope change with placebo kink points, and thus have a small KP randomization p -value. If, on the other hand, we falsely specify a quadratic function with no kink as a discontinuous slope change, we would observe discernible kink estimates with placebo kink points and a large KP randomization p -value.

Table 1: Herbicide Exposure and Population Size in 2001 and 2020

	Panel A: ln HERB				
	(1)	(2)	(3)	(4)	(5)
First stage					
EdgeDist $\times \mathbb{1}[\text{EdgeDist} \geq 0]$	-0.693*** (0.095)	-0.660*** (0.089)	-0.629*** (0.087)	-0.633*** (0.086)	-0.632*** (0.084)
<i>F</i> -statistic (weak instrument)	53.132	54.585	51.893	54.03	56.504
Adjusted R ²	0.620	0.652	0.663	0.666	0.677
Randomization inference					
Running variable (RV) randomization <i>p</i> -value	0.000	0.000	0.000	0.000	0.000
Spatial noise (SN) randomization <i>p</i> -value	0.000	0.000	0.000	0.000	0.000
	Panel B: ln Population (2001)				
	(1)	(2)	(3)	(4)	(5)
Second stage					
ln HERB	-0.203*** (0.069)	-0.177*** (0.065)	-0.168*** (0.063)	-0.165*** (0.063)	-0.165*** (0.064)
10% increase effect size	-1.93%	-1.69%	-1.6%	-1.57%	-1.58%
Average outcome	1.315	1.315	1.315	1.315	1.315
Randomization inference (reduced form)					
Kink point (KP) randomization <i>p</i> -value	0.019	0.021	0.004	0.003	0.000
RV randomization <i>p</i> -value	0.003	0.003	0.006	0.007	0.007
SN randomization <i>p</i> -value	0.004	0.004	0.005	0.006	0.006
	Panel C: ln Population (2020)				
	(1)	(2)	(3)	(4)	(5)
Second stage					
ln HERB	-0.294*** (0.076)	-0.264*** (0.072)	-0.258*** (0.072)	-0.254*** (0.072)	-0.255*** (0.072)
10% increase effect size	-2.8%	-2.51%	-2.45%	-2.42%	-2.43%
Average outcome	1.467	1.467	1.467	1.467	1.467
Randomization inference (reduced form)					
KP randomization <i>p</i> -value	0.013	0.007	0.008	0.009	0.004
RV randomization <i>p</i> -value	0.000	0.000	0.000	0.000	0.001
SN randomization <i>p</i> -value	0.000	0.000	0.000	0.000	0.000
Observations	522	522	522	522	522
Avg. N neighbors (Conley SE cluster size)	27.4	27.4	27.4	27.4	27.4
Key target covariates	✓	✓	✓	✓	✓
Geographic covariates		✓	✓	✓	✓
Historical covariates			✓	✓	✓
ln spatially-lagged HERB					✓
Fixed effects and $f(\text{Lon}, \text{Lat})$	✓	✓	✓	✓	✓

Notes: * $p < 0.1$; ** $p < 0.05$; *** $p < 0.01$. Conley (1999) standard errors adjusted for spatial clustering with a 30 km cutoff and a Bartlett kernel are in parentheses. Key target covariates: NVA base distance, population (1967–1969), U.S. base distance, U.S. troop distance, rice cropland, road distance, slash and burn cropland, Viet Cong control prevalence. Geographic covariates: Precipitation, wind speed, elevation, flow accumulation, forest presence, rice suitability, river distance, ruggedness. Historical covariates: Bombing point distance, border distance, number of neighbor hamlets, railway distance. ln spatially-lagged HERB is the logged average HERB among the neighbor hamlets with a 30 km cutoff. Fixed effects: Agent fixed effect, district fixed effect, end-edge fixed effect, pre-1967 mission fixed effect. Randomization inference: KP randomization *p*-value is computed by the permutation test of Ganong and Jäger (2018) with 10,000 placebo kink points drawn from uniform distribution $\mathcal{U}(-4 \text{ km}, 4 \text{ km})$. RV randomization *p*-value is obtained by randomly assigning the running variable to the sample hamlets for 10,000 times. SN randomization *p*-value is obtained by 10,000 synthetic spatial noise simulations of Kelly (2021) with the outcome replaced by randomly generated spatial noise.

ization inference is to randomly assign the running variable (RV) and the corresponding treatment-side indicator variable to the sample hamlets while holding the kink point fixed (e.g., [Dell and Querubin, 2018](#), 30–33; see also, [Cattaneo, Frandsen, and Titiunik, 2015](#)). The RV randomization two-sided p -values report the share of the absolute 10,000 placebo coefficients that are larger than the absolute actual reduced-form kink coefficient. Finally, to address potential spatial curve-fitting and residual spatial autocorrelation, we use the spatial noise (SN) randomization inference procedure developed by [Kelly \(2021\)](#). The SN randomization inference procedure replaces the outcome by synthetic noise with the same estimated spatial structure of the observed outcome partialled out by covariates. If the estimation is not an artifact of spatial trends, the observed variable should not explain spatial noise. The SN randomization p -value indicates the fraction of 10,000 spatial noise simulations which yield absolute t values greater than the absolute t value estimated with the observed data.

For both treatment and outcomes, the randomization inference results are consistent with asymptotic inference. The three series of randomization p -values remain smaller than the conventional 5% threshold, suggesting that the actual estimates are unlikely to arise from misspecification of the underlying nonlinearity (KP randomization), random chance (RV randomization), or spatial autocorrelation and curve-fitting (SN randomization).

Turning to magnitude, the coefficient estimates can readily be interpreted as elasticity given the log-log specification. The estimates suggest that, measured at the 100 meter grid scale, a 10% increase in herbicide exposure is persistently followed by a 2.42% ($-0.254 \times \ln(1.1) = 0.0242$, Model 4, with all covariates) to 2.8% (Model 1, without covariates) decrease in population size in 2020 (Panel B), and a 1.57% to 1.93% decrease in 2001 (Models 1 and 4 in Panel C). Note that the 10% increase reference does not overstate the magnitude of the treatment effect, as such an increase in herbicide exposure is observed within a geographically small area around the kink edges. Specifically, a 10.8% increase in the treatment approximately corresponds to the difference in \ln HERB between the average of the control hamlets within a 500 meter distance (250 meters on each side) from the kink

edge with the average of the treated hamlets within the same distance from the kink edge.

Besides the baseline population growth during the 2001–2020 period (from 1.315 to 1.467 in the logarithm scale, Table 1), the growing, rather than fading away, coefficient size implies that herbicide legacies shape not only population *size* but also population *growth rate*. This leads to a testable implication that a similar negative association is also present in local population growth rate, which contrasts the conventional wisdom of rapid recovery of population from wartime destruction.

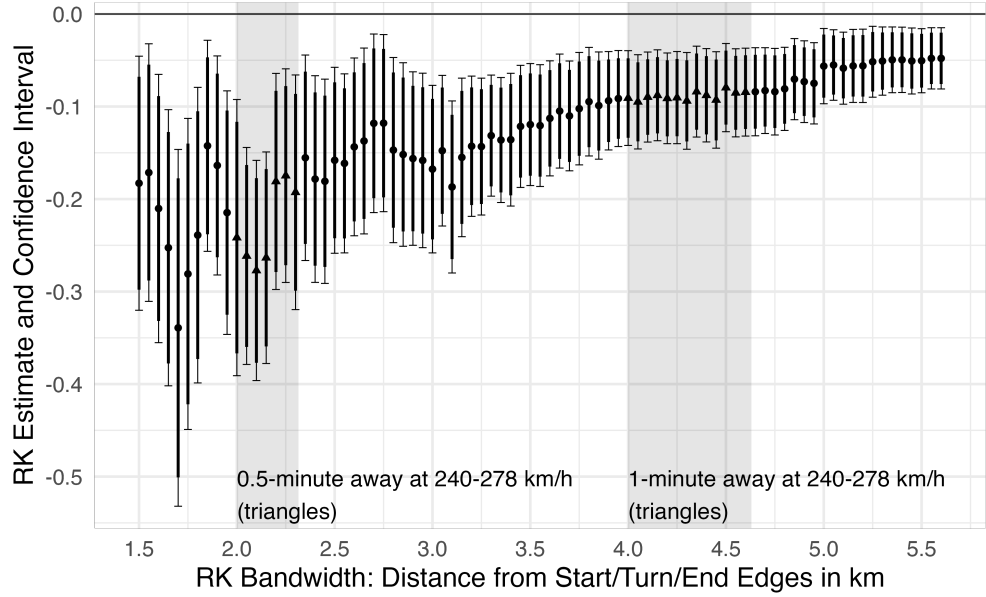
4.2 Population Growth Rate Estimates

To examine the testable implication of cumulatively increasing legacies of herbicide exposure, we reestimate the RK models with the overall and annual population growth rates during the 2001–2020 period as the outcomes, using both cross-sectional and panel setups. This growth-rate specification also surmounts the robustness concern that a small number of volatile and less persistent population count observations in 2001 and 2020 drive the estimation results. For the panel specification, we extend the baseline cross-sectional specification by replacing the outcome by the annual growth rate and adding a year fixed effect as an additional control.²³ In the panel setup, we report robust standard errors clustered at the hamlet level. Another robustness issue remaining in Table 1 is that the results are based on a fixed bandwidth of 4 km, leaving potential concern for the bandwidth choice driving the results. To examine the herbicide legacies on population growth rate and address these robustness concerns, we report the RK estimates for overall and annual population growth rates across different RK bandwidths ranging from 1.5 km to 5.6 km with an increment of 50 meters.

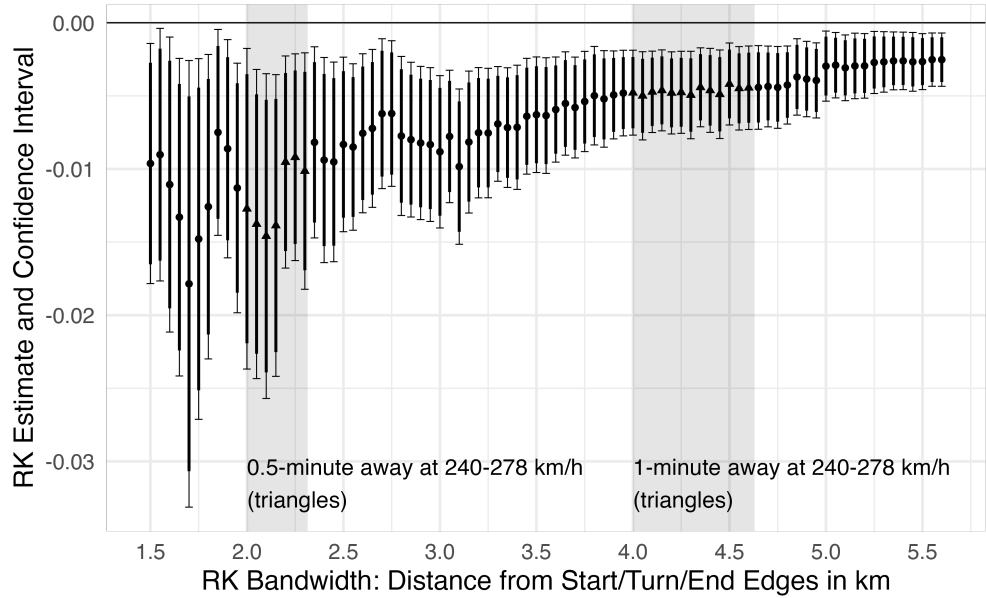
Figure 4 presents the RK estimates for overall (Panel (a)) and annual (Panel (b)) population growth rates across bandwidth sizes. Regardless of the bandwidth settings and outcomes, the growth rate estimates reveal a negative association consistent with the population size estimates.²⁴ The effect size is also discernible given the average outcome of

²³The results remain qualitatively unchanged when further adjusting for the lagged outcome, Y_{hdt-1} .

²⁴Figure 4 follows the specification of model (1) in Table 1 (without covariate adjustments). Note that,



(a) Overall Population Growth Rate, 2001–2020



(b) Annual Population Growth Rate, 2002–2020

Figure 4: Herbicide Exposure and Population Growth Rate

Notes: Symbols and thin (thick) vertical segments with horizontal ticks represent the RK estimates and the corresponding 95% (90%) confidence intervals based on Conley (1999) standard errors with spatial clustering (Panel (a)) and robust standard errors with hamlet-level clustering (Panel (b)). The model specification in Panel (a) follows model (1) in Table 1. Panel (b) adds a year fixed effect to the baseline specification. Grey shades represent “0.5-minute-away” (2–2.315 km) and “one-minute-away” distances (4–4.63 km) from the kink point at the typical airspeed of Ranch Hand aircraft of 240–278 km/h, and triangles indicate the corresponding point estimates. Annual growth estimate in Panel (b) covers the 2002–2020 period as the outcome is defined as $\ln \text{Population}_t - \ln \text{Population}_{t-1}$ and our dataset covers the 2001–2020 period.

0.151 (or $e^{0.151} = 1.163$, 16.3% overall population growth in 2001–2020) and the geographically small level of measurement of 100 meter grid. The cross-sectional RK estimate of $\tau = -0.091$ with the baseline bandwidth of 4 km (a “one-minute-away” distance) suggests that a 10% increase in herbicide exposure translates into a 0.87% decrease ($-0.091 \times \ln(1.1) = -0.0087$) in the overall (logged) population growth rate in 2001–2020 (Figure 4(a)). Given $\ln \text{Population}_{2020} - \ln \text{Population}_{2001} \approx \frac{\text{Population}_{2020}}{\text{Population}_{2001}} - 1$, a 0.87% decrease can approximately be interpreted as the effect size in the percentage point scale. The negative association is also visible in the panel specification with the annual population growth rate as the outcome (Figure 4(b)), revealing the herbicide legacies remaining in the dynamics as well as the snapshots of population outcomes in Vietnam in the present day.

4.3 Robustness Check and Sensitivity Analysis

Robustness and sensitivity concerns remaining in the main estimates include the robustness to the parameter choice to construct the RK sample and the exposure score, HERB, confounding kink in observed covariates and model dependence, and unobserved confounding kink. In addition to the placebo kink (covariate kink) estimates reported above, Appendix C addresses these concerns by leveraging alternative combinations of flight buffer width and half-decay distance parameters, all possible $2^N \text{ covariates} = 2^{20} = 1,048,576$ model specifications per outcome, a jackknife approach and the known historical differences in counterinsurgency strategies across four U.S. Corps Tactical Zones in South Vietnam (see, e.g., Dell and Querubin, 2018), and a sensitivity analysis approach to quantify how severe unobserved confounding forces would need to be to eliminate the main estimates (Cinelli and Hazlett, 2020). Reassuringly, none of the robustness checks yield results that would invalidate or overturn the main findings.

as reported in Appendix C.1, the growth rate specification is remarkably robust to different model specifications (different combinations of adjusted covariates) and exhibits little model dependence. The empirical distribution of the RK estimates of all possible $2^N \text{ covariates} = 2^{20} = 1,048,576$ model specifications is almost normally distributed with the mean and median estimates of 0.091 (Appendix Figure C.1), which is nearly identical to the point estimate reported in the text and Figure 4(a) ($\hat{\tau} = 0.091$).

5 Conclusion

This article combined the historical records of herbicide missions with a fuzzy RK design and revealed the negative legacies of herbicidal warfare on contemporary population size and growth rate in Vietnam. The empirical analysis suggests that the temporary shock of herbicidal warfare left lasting, rather than temporary, effects on contemporary population outcomes. While the reported results tell us little about the underlying mechanisms, there are at least three distinct, although not mutually exclusive, explanations for the revealed persistent association, which also opens up pathways for future research. First, the negative association might reflect decreased birthrates and life expectancy. The reported negative association between herbicide exposure and health outcomes (e.g., Le, Pham, and Polacheck, 2022; Vuong, 2024; Yamashita and Trinh, 2022) makes the heavily sprayed areas persistently suffer lower birthrates and decreased life expectancy. Second, and relatedly, the lower population size and growth rates can arise from deteriorated agricultural productivity to sustain local population (e.g., Appau, Churchill, Smyth et al., 2021). Finally, domestic migration preferences and patterns can also shape population dynamics. Increased out-migration from the herbicide affected areas coupled with decreased in-migration into the damaged areas can also account for the lasting negative associations.

References

- Altonji, Joseph G., and Rosa L. Matzkin. 2005. Cross section and panel data estimators for nonseparable models with endogenous regressors. *Econometrica* 73 (4):1053–1102.
- Ando, Michihito. 2017. How much should we trust regression-kink-design estimates? *Empirical Economics* 53 (3):1287–1322.
- Appau, S, S A Churchill, R Smyth, and T A Trinh. 2021. The long-term impact of the Vietnam War on agricultural productivity. *World Development* 146 (October):105,613.
- Bana, Sarah H., Kelly Bedard, and Maya Rossin-Slater. 2020. The Impacts of Paid Family Leave Benefits: Regression Kink Evidence from California Administrative Data. *Journal of Policy Analysis and Management* 39 (4):888–929.
- Bauer, Michal, Christopher Blattman, Julie Chytilová, Joseph Henrich, Edward Miguel, and Tamar Mitts. 2016. Can War Foster Cooperation? *Journal of Economic Perspectives* 30 (3):249–274.
- Berman, Chantal, Killian Clarke, and Rima Majed. 2023. From Victims to Dissidents: Legacies of Violence and Popular Mobilization in Iraq (2003-2018). *American Political Science Review* forthcoming.
- Blattman, Christopher. 2009. From Violence to Voting: War and Political Participation in Uganda. *American Political Science Review* 103 (2):231–247.
- Bosker, Maarten, Steven Brakman, Harry Garretsen, and Marc Schramm. 2007. Looking for multiple equilibria when geography matters: German city growth and the WWII shock. *Journal of Urban Economics* 61 (1):152–169.
- Brakman, Steven, Harry Garretsen, and Marc Schramm. 2004. The strategic bombing of German cities during World War II and its impact on city growth. *Journal of Economic Geography* 4 (2):201–218.
- Buckingham, William A. 1982. *Operation Ranch Hand: The Air Force and Herbicides in Southeast Asia, 1961-1971*. Washington, DC: Office of Air Force History.
- Calonico, Sebastian, Matias D. Cattaneo, and Rocío Titiunik. 2015. Optimal Data-Driven Regression Discontinuity Plots. *Journal of the American Statistical Association* 110 (512):1753–1769.
- Card, David, Andrew Johnston, Pauline Leung, Alexandre Mas, and Zhuan Pei. 2015. The effect of unemployment benefits on the duration of unemployment insurance receipt: New evidence from a regression kink design in Missouri, 2003-2013. *American Economic Review* 105 (5):126–130.
- Card, David, David Lee, Zhuan Pei, and Andrea Weber. 2012. Nonlinear Policy Rules and the Identification and Estimation of Causal Effects in a Generalized Regression Kink

Design.

- Card, David, David S. Lee, Zhuan Pei, and Andrea Weber. 2015. Inference on Causal Effects in a Generalized Regression Kink Design. *Econometrica* 83 (6):2453–2483.
- . 2017. Regression Kink Design: Theory and Practice. In *Regression Discontinuity Designs: Theory and Applications*, edited by Matias D. Cattaneo and Juan Carlos Escanciano. Bingley: Emerald Publishing.
- Cattaneo, Matias D., Brigham R. Frandsen, and Rocío Titiunik. 2015. Randomization Inference in the Regression Discontinuity Design: An Application to Party Advantages in the U.S. Senate. *Journal of Causal Inference* 3 (1):1–24.
- Cattaneo, Matias D., Michael Jansson, and Xinwei Ma. 2020. Simple Local Polynomial Density Estimators. *Journal of the American Statistical Association* 115 (531):1449–1455.
- Cinelli, Carlos, and Chad Hazlett. 2020. Making sense of sensitivity: Extending omitted variable bias. *Journal of the Royal Statistical Society. Series B: Statistical Methodology* 82 (1):39–67.
- Conley, Timothy G. 1999. GMM estimation with cross sectional dependence. *Journal of Econometrics* 92 (1):1–45.
- Davis, Donald R., and David E. Weinstein. 2002. Bones, Bombs, and Break Points: The Geography of Economic Activity. *American Economic Review* 92 (5):1269–1289.
- . 2008. A search for multiple equilibria in urban industrial structure. *Journal of Regional Science* 48 (1):29–65.
- Defense Digital Service. 2016. Theater History of Operations Data (THOR): Vietnam War. Available at: <https://data.world/datamil/vietnam-war-thor-data>.
- Dell, Melissa, and Pablo Querubin. 2018. Nation Building Through Foreign Intervention: Evidence from Discontinuities in Military Strategies. *Quarterly Journal of Economics* 133 (2):701–764.
- Douglass, Rex W. 2011. Data of the Vietnam War v1.0 (Vietnam Hamlet Evaluation System Gazeteer Data). Available at: <https://esoc.princeton.edu/data/vietnam-hamlet-evaluation-system-gazetteer-data>, accessed July 7, 2021.
- Fick, Stephen E., and Robert J. Hijmans. 2017. WorldClim 2: New 1-km spatial resolution climate surfaces for global land areas. *International Journal of Climatology* 37 (12):4302–4315.
- Florens, J.P., J.J. Heckman, C Meghir, and E. Vytlacil. 2008. Identification of Treatment Effects Using Control Functions in Models With Continuous, Endogenous Treatment and Heterogeneous Effects. *Econometrica* 76 (5):1191–1206.
- Ganong, Peter, and Simon Jäger. 2018. A Permutation Test for the Regression Kink Design. *Journal of the American Statistical Association* 113 (522):494–504.

- Gilligan, Michael J., Benjamin J. Pasquale, and Cyrus Samii. 2014. Civil war and social cohesion: Lab-in-the-field evidence from Nepal. *American Journal of Political Science* 58 (3):604–619.
- Grasse, Donald. 2023. State Terror and Long-Run Development: The Persistence of the Khmer Rouge. *American Political Science Review* forthcoming.
- Institute of Medicine (Committee to Review the Health Effects in Vietnam Veterans of Exposure to Herbicides). 1995. *Veterans and Agent Orange: Health Effects of Herbicides Used in Vietnam*. Washington, D.C.: National Academy Press.
- Kelly, Morgan. 2021. Persistence, Randomization, and Spatial Noise. *CEPR Discussion Paper* DP16609.
- Landais, Camille. 2015. Assessing the welfare effects of unemployment benefits using the regression kink design. *American Economic Journal: Economic Policy* 7 (4):243–278.
- Le, Duong Trung, Thanh Minh Pham, and Solomon Polacheck. 2022. The long-term health impact of Agent Orange: Evidence from the Vietnam War. *World Development* 155:105,813.
- Lehner, Bernhard, Kristine Verdin, and Andy Jarvis. 2008. New global hydrography derived from spaceborne elevation data. *Eos* 89 (10):93–94.
- Lichter, Andreas, Max Löffler, and Sebastian Siegloch. 2020. The Long-Term Costs of Government Surveillance: Insights from Stasi Spying in East Germany. *Journal of the European Economic Association* 19 (2):741–789.
- Lin, Erin. 2022. How War Changes Land: Soil Fertility, Unexploded Bombs, and the Underdevelopment of Cambodia. *American Journal of Political Science* 66 (1):222–237.
- McCormick, John T. 2021. The Hamlet Evaluation System Reevaluated. Available at: https://github.com/jtmccorm/HES_Reevaluated, accessed July 7, 2021.
- Miguel, Edward, and Gérard Roland. 2011. The long-run impact of bombing Vietnam. *Journal of Development Economics* 96 (1):1–15.
- Military Assistance Command, Vietnam (MACV). 1969. Military Operations: Herbicide Operations (U). APO San Francisco 96222, Accession Number: AD0779793. Available at: <https://apps.dtic.mil/sti/citations/AD0779793>, accessed July 10, 2023.
- National Academy of Sciences. 1974. *The Effects of Herbicides in South Vietnam: Part A Summary and Conclusions*. Washington, DC: National Academy of Sciences.
- Nunn, Nathan, and Leonard Wantchekon. 2011. The slave trade and the origins of Mistrust in Africa. *American Economic Review* 101 (7):3221–3252.
- Palmer, Michael, Cuong Viet Nguyen, Sophie Mitra, Daniel Mont, and Nora Ellen Groce. 2019. Long-lasting consequences of war on disability. *Journal of Peace Research* 56 (6):860–875.

- Pei, Zhuan, David S. Lee, David Card, and Andrea Weber. 2022. Local Polynomial Order in Regression Discontinuity Designs. *Journal of Business and Economic Statistics* 40 (3):1259–1267.
- Riaño, Juan Felipe, and Felipe Valencia Caicedo. 2024. Collateral Damage: The Legacy of the Secret War in Laos. *Economic Journal* forthcoming.
- Rowley, Ralph A. (Office of Air Force History). 1975. The Air Force in Southeast Asia: FAC Operations, 1965–1970. Office of Air Force History, May 1975, available at: <https://media.defense.gov/2011/Mar/24/2001330117/-1/-1/0/AFD-110324-008.pdf>.
- Singhal, Saurabh. 2019. Early life shocks and mental health: The long-term effect of war in Vietnam. *Journal of Development Economics* 141 (March):102,244.
- Stellman, Jeanne Mager, Steven D. Stellman, Richard Christian, Tracy Weber, and Carrie Tomasallo. 2003. The extent and patterns of usage of agent orange and other herbicides in Vietnam. *Nature* 422 (6933):681–687.
- Stellman, Jeanne Mager, Steven D. Stellman, Tracy Weber, Carrie Tomasallo, Andrew B. Stellman, and Richard Christian. 2003. A geographic information system for characterizing exposure to Agent Orange and other herbicides in Vietnam. *Environmental Health Perspectives* 111 (3):321–328.
- Stellman, Steven D., and Jeanne M. Stellman. 1986. Estimation of exposure to agent orange and other defoliants among american troops in vietnam: A methodological approach. *American Journal of Industrial Medicine* 9 (4):305–321.
- U.S. Geological Survey (USGS). 1996. Global 30-Arc-Second Elevation Data, GTOPO30.
- Vuong, Dinh Tuan Nguyen. 2024. The Persistent Health Effects of Defoliating Vietnam.
- Yamada, Takahiro, and Hiroyuki Yamada. 2021. The long-term causal effect of U.S. bombing missions on economic development: Evidence from the Ho Chi Minh Trail and Xieng Khouang Province in Lao P.D.R. *Journal of Development Economics* 150 (October):102,611.
- Yamashita, Nobuaki, and Trong Anh Trinh. 2022. Long-Term Effects of Vietnam War: Agent Orange and the Health of Vietnamese People After 30 Years. *Asian Economic Journal* 36 (2):180–202.
- Zabel, Florian, Birgitta Putzenlechner, and Wolfram Mauser. 2014. Global agricultural land resources: A high resolution suitability evaluation and its perspectives until 2100 under climate change conditions. *PLoS ONE* 9 (9):1–12.

ONLINE APPENDIX FOR “NOT GONE WITH THE WIND: LONG-RUN IMPACTS OF HERBICIDAL WARFARE IN VIETNAM”

Gaku Ito* Duc Tran† Yuichiro Yoshida‡

May 7, 2024

Contents

A Data Details	A1
A.1 Descriptive Statistics	A1
A.2 Stellman-National Academy of Sciences HERBS File	A1
A.3 Running Variable Coding Procedure	A3
A.4 Historical Maps and Archival Sources	A4
A.5 Naive OLS Estimates	A7
B Identification Assumption	A8
B.1 Running Variable Distribution	A8
B.2 Covariate Distribution	A9
C Robustness Check	A12
C.1 Confounding Nonlinearity and Model Dependence	A12
C.2 Flight Buffer Width and Half-Decay Distance	A15
C.3 Counterinsurgency Strategy and Jackknife Estimates	A16
C.4 Unobserved Confounding Forces and Sensitivity Analysis	A18
References	A19

*Associate Professor, Graduate School of Economics, Osaka Metropolitan University. 3-3-138 Sugimoto, Sumiyoshi, Osaka 558-8585, Japan. Email: gaku@omu.ac.jp. URL: <https://gaku-ito.github.io>.

†Research Fellow, Graduate School of Integrated Sciences for Life, Hiroshima University. 1-4-4 Kagamiyama, Higashi-Hiroshima, Hiroshima 739-8528, Japan. Email: tranduc@hiroshima-u.ac.jp. URL: <https://ductran-data.github.io>.

‡Professor, School of Economics, Kwansei Gakuin University. 1-155 Uegahara Ichiban-cho, Nishinomiya 662-8501, Japan. Email: yuichiroyoshida@kwansei.ac.jp.

A Data Details

A.1 Descriptive Statistics

Table A.1 reports the summary statistics of the variables used in the empirical analysis. Nonbinary variables excepting the running variable, Viet Cong control prevalence, and population growth rates are log-transformed.

A.2 Stellman-National Academy of Sciences HERBS File

The key source of our empirical analysis is the Stellman-National Academy of Sciences (NAS) version of the Herbicide Report System (HERBS) file (S-NAS HERBS, [Stellman, Stellman, Christian et al., 2003](#); [Stellman, Stellman, Weber et al., 2003](#)). We first web-scraped the records in the database from the Agent Orange Warehouse website.¹ We then converted the geocoordinate information originally recorded in the military grid reference system (MGRS) format into the longitude-latitude format, and combined the converted geocoordinates with other mission- and flight-level information.

In addition to the geocoordinates of spray start, turn, end points, the database contains information about the mission dates, spray methods, and agents and gallons sprayed in individual missions.² The spray method is categorized into “Fixed-Wing Aircraft,” “Ground Spraying,” “Helicopter,” and “Unspecified” categories. As [Stellman, Stellman, Weber et al. \(2003, 323\)](#) note, a majority of herbicide missions was carried out by fixed-wing aircraft (C-123 airplanes), with 5,961 (65.2%) out of 9,141 missions recorded as aircraft missions. The remaining 3,180 missions include 2,108 (23.1%) missions by helicopters, 446 (4.9%) ground applications, and 626 (6.8%) missions with the method information remaining unspecified. As explained in the main text, our empirical analysis uses the fixed-wing aircraft missions by the US Air Force, which dispersed approximately 95% of all herbicides ([Stellman, Stellman,](#)

¹ Available at: <http://www.workerveteranhealth.org/milherbs/new/>, accessed August 29, 2021.

² For the aircraft navigation system in the 1960s and the development of the tactical air navigation system (TACAN) distance measuring equipment (DME) in the region, see, for example, [Rowley \(1975\)](#).

Table A.1: Descriptive Statistics

	Observations	Mean	SD	Median	IQR
Panel A: Dependent Variables					
Population (2001)	716	1.333	0.995	1.193	1.327
Population (2020)	716	1.484	1.109	1.287	1.324
Overall Population Growth Rate (2001–2020)	716	0.152	0.319	0.095	0.338
Annual Population Growth Rate (2001–2020)	13,604	0.008	0.104	0.003	0.074
Panel B: Treatment and Assignment Variables					
HERB ($D^{\text{Half}} = 500\text{m}$)	716	7.093	1.946	7.488	2.411
Edge Distance	716	-1.140	2.924	-1.418	4.660
$\mathbb{1}[\text{EdgeDist}_{ij} \geq 0]$	716	0.330	0.470	0.000	1.000
Panel C: Covariates					
Key Target Covariates					
North Vietnam Army Base Distance	716	2.758	0.730	2.844	1.059
U.S. Base Distance	716	2.996	0.820	3.149	1.065
U.S. Troop Distance	716	4.892	1.276	5.220	1.778
Population (1967–1969)	716	3.143	3.314	0.693	6.524
Rice Cropland	716	0.300	0.459	0.000	1.000
Road Distance	716	1.463	1.529	1.671	2.248
Slash and Burn Cropland	716	0.251	0.434	0.000	1.000
Viet Cong Control Prevalence	716	0.172	0.325	0.000	0.129
Geographic Covariates					
Elevation	716	4.319	1.454	3.850	2.918
Flow Accumulation	716	1.747	2.280	0.693	2.996
Forest Presence	716	0.522	0.500	1.000	1.000
Precipitation	716	7.464	0.200	7.446	0.315
Rice Suitability	716	1.619	1.322	1.099	3.258
River Distance	716	-0.199	1.336	-0.068	1.719
Ruggedness	716	1.072	0.786	0.693	0.916
Wind Speed	716	0.778	0.177	0.771	0.314
Historical Covariates					
Bombing Point Distance	716	-0.190	0.822	-0.168	1.215
Border Distance	716	4.330	0.828	4.554	0.798
Number of Neighbor Hamlets	716	2.997	0.879	3.045	1.153
Railway Distance	716	2.992	1.632	3.364	2.069
Geocoordinates					
Longitude	716	107.911	1.004	108.222	1.686
Latitude	716	13.177	2.081	13.610	3.510

Notes: SD = standard deviation, IQR = interquartile range.

Christian et al., 2003, 681–682; see also, Figure 1 in the main text).

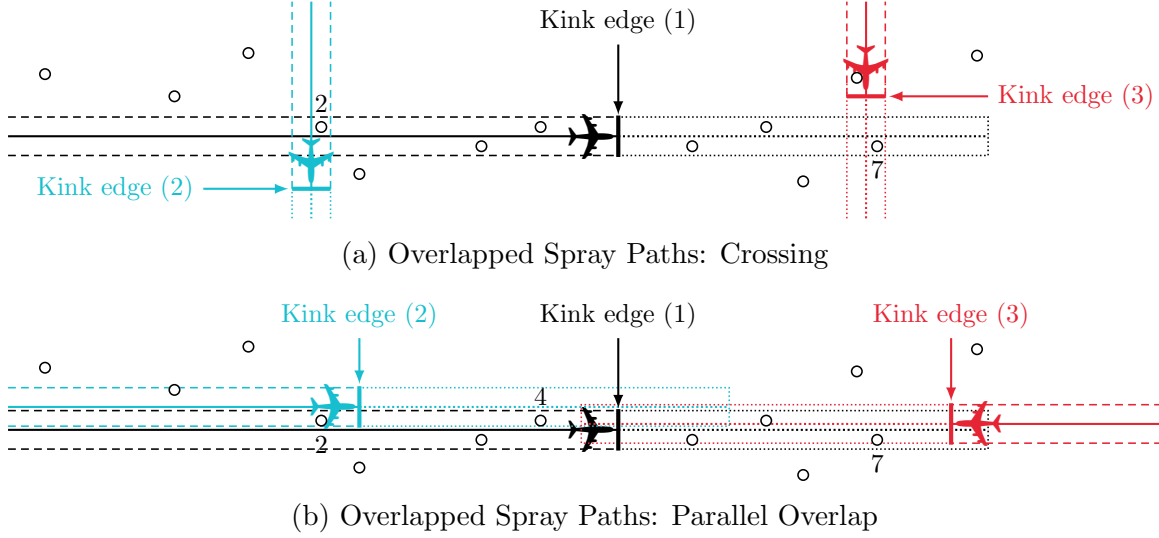


Figure A.1: Running Variable Coding with Overlapped Spray Paths

Notes: (a), (b) Dashed and dotted segments represent distinct spray path polygons. Hamlets 2 and 7 are geographically covered by multiple spray path polygons.

A.3 Running Variable Coding Procedure

The main text explains the coding procedure of the running variable with examples in which single flight path polygons cover individual hamlets. When multiple flight polygons cover single hamlets, we adopt group-specific rules to measure the kink edge distance as illustrated by Figure A.1. For the treatment group hamlets, we first take the minimum distance to the kink edges and then assign the maximum, instead of the minimum, of the distance measures as its running variable. For example, we assign the distance to kink edge (1) instead of the distance to kink edge (2) as the running variable for hamlet 2 (in the treatment group). For the control group hamlets, we first measure the distances to the kink edges of all flight polygons covering the hamlets, and then assign the minimum distance as its running variable. For example, the running variable for hamlet 7 (in the control group) in Figure A.1(a) is measured as the distance to kink edge (3) instead of the distance to kink edge (1).

We adopt these group-specific coding rules because the coding procedure for the control hamlets might underestimate the kink-edge distance for the treated hamlets. As illustrated by hamlet 2 in Figure A.1(a), when covered by multiple flight path polygons, a treated

hamlet may be located in the middle of one flight polygon (e.g., 4 km from kink edge 1) while located closed to the kink edges of another flight path polygon (e.g., 250 meters from kink edge 2). In this case, a simple minimum distance coding assigns 250 meters to hamlet 2 as the running variable. However, this coding significantly underestimates the hamlet's distance to kink edge because the hamlet is located in the middle of another flight path and is strongly exposed to the treatment due to the mission flight with kink edge (1) regardless of its distance to kink edge (2). Our coding rule prevents this underestimation of the running variable and assigns 4 km instead of 250 meters to the treated hamlet.

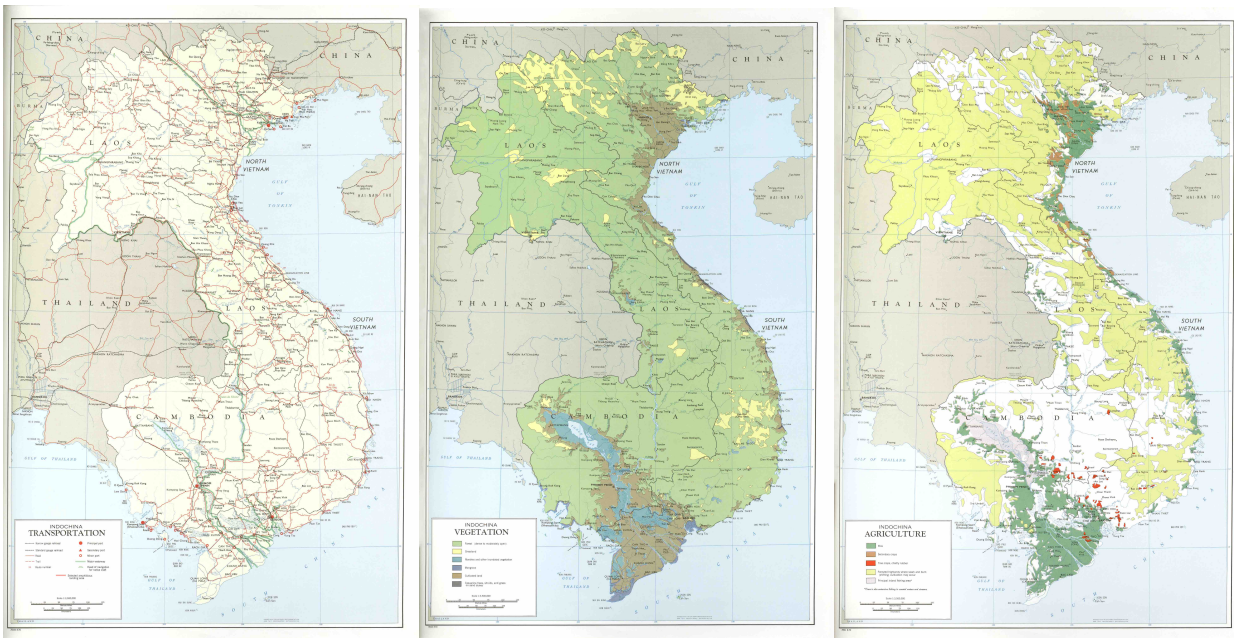
Instead of the maximum-of-minimum distance rule for the treated hamlets, we rely on the minimum-of-minimum distance rule for the control group hamlets (e.g., hamlet 7). Because the control group hamlets are located outside of the flight polygons, their proximity to the kink edges can best be measured by the minimum distance. In the case of hamlet 7, we assign the distance to kink edge 3 as the running variable. Figure A.1(b) illustrates another example with multiple spray paths with parallel overlaps. The kink edge distances for hamlets 2 and 7 are measured in the same manner as illustrated with the case of Figure A.1(a) (i.e., distance to kink edge 1 for hamlet 2, and distance to kink edge 3 for hamlet 7).

A.4 Historical Maps and Archival Sources

As explained in the main text, some of our covariates relies on historical maps and archival sources. As one of the key sources, we originally georeferenced and image-processed the historical maps of *Indochina Atlas* published by the Central Intelligence Agency (CIA) in 1970 and later digitized by the University of Texas Libraries.³ As shown in Figures A.2(a) to A.2(c), the *Atlas* provides a series of maps as of the period including the transportation lines (i.e., roads, trails, and railways), surface configurations, and crop fields. Figures A.2(d) to (f) show the image-processed results for transportation lines, forest coverage, and croplands.⁴

³The digitized (scanned) maps are available at https://maps.lib.utexas.edu/maps/indochina_atlas/ and <https://www.history.navy.mil/research/library/exhibits/maps/indochina-atlas-1970.html>.

⁴For image-processing, we primarily rely on the mean-shift segmentation algorithm implemented in Orfeo Toolbox (Grizonnet, Michel, Poughon et al., 2017) and the skeletonization algorithm of Tveite (2015). We



(a) Transportation Map

(b) Vegetation Map

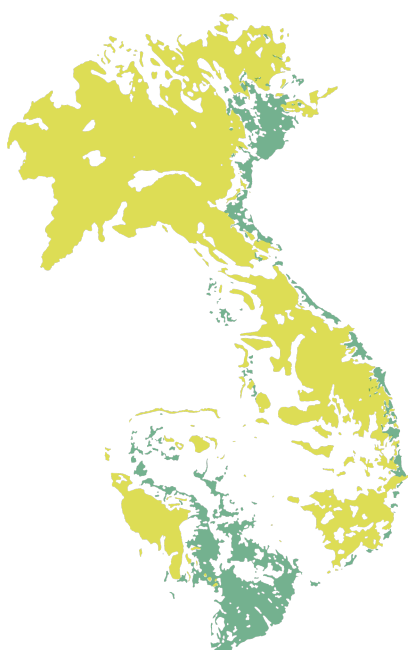
(c) Agriculture Map



(d) Road and Railway Network



(e) Forest Coverage



(f) Rice Croplands and Slash and Burn Cultivation Areas

Figure A.2: *Indochina Atlas* Maps and the Image-Processed Vector Objects

Notes: Panels (a), (b), and (c) depict the original (non-georeferenced) scanned maps of *Indochina Atlas*, digitized by the University of Texas Libraries. Panels (d), (e), and (f) show the generated vector objects (lines and polygons). Red and black segments in Panel (d), respectively, indicate roads (including trails) and railways. Green region in Panel A.2(e) represents forest presence. In Panel (f), green regions represent rice croplands, and yellow regions indicate the areas with slash and burn cultivation.

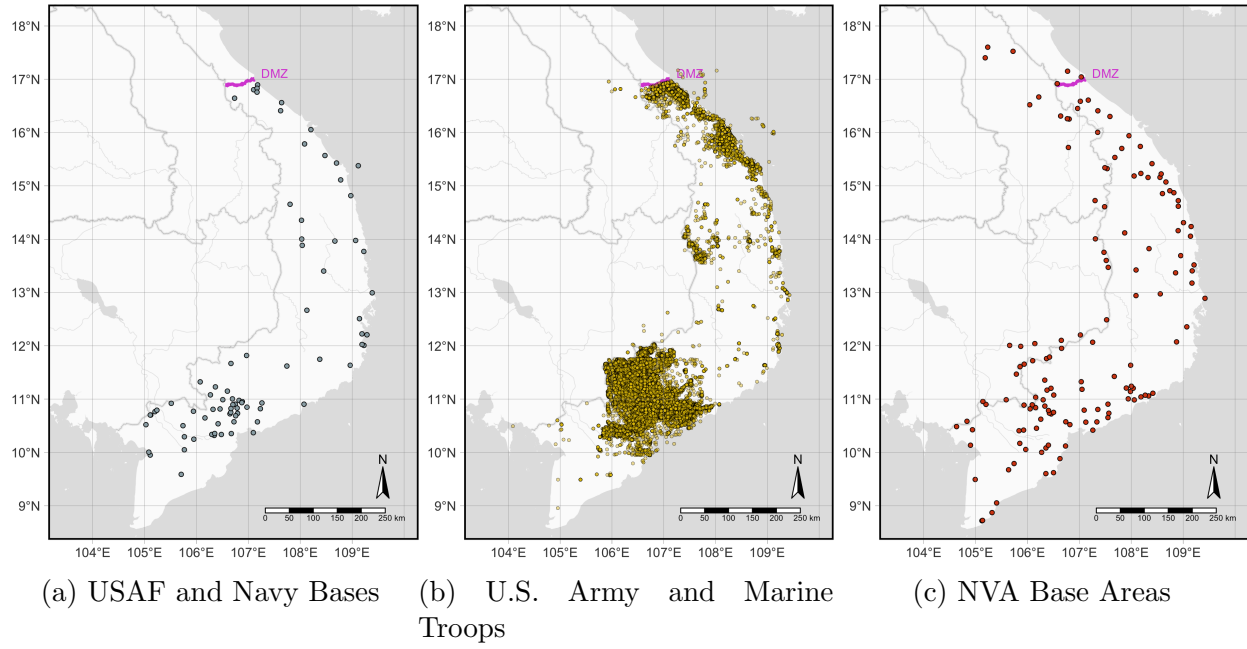


Figure A.3: Locations of U.S. Bases, Troops, and NVA Base Areas

Notes: Dots in each panel indicate, respectively, (a) U.S. Air Force and Navy bases, (b) U.S. Army and Marine troop locations, and (c) suspected areas of North Vietnam Army (NVA) base areas in and near South Vietnam. Dots in (c) represent the geocoordinates of the “approximate center” of the suspected NVA base areas (National Archives and Records Administration. 2007. “Reference Copy of Technical Documentation for Accessioned Electronic Records: Enemy Base Area File (BASFA), 7/1967–7/1971, Translation File, RG 330, Records of the Office of the Secretary of Defense.” pp.26–27. Available at: <https://catalog.archives.gov/id/2573252>, accessed June 16, 2023).

We rely on several other sources to measure the historical landscape of military bases and troops. Suspected areas of North Vietnam Army (NVA) base are retrieved from the Enemy Base Area File (BASFA), July 1, 1967–July 1, 1971 hosted by the National Archives and Records Administration (NARA).⁵ The locations of U.S. Air Force and Navy bases and U.S. Army and Marine troops are retrieved from the S-NAS HERBS database. Figure A.3 depicts the spatial distributions of U.S. bases, U.S. troop locations, and the suspected areas of NVA bases in and near South Vietnam.

rely on the same image-processing procedures to generate the polygons of demarcation line and demilitarized zone (DMZ) from CIA’s “Vietnam demarcation line and demilitarized zone. 12-66” map as of 1966 (<https://www.loc.gov/resource/g8021f.ct002840/>, accessed September 22, 2021).

⁵National Archival Identifier 2573252; Accession Number of NN3-330-76-037. Available at: <https://catalog.archives.gov/id/2573252>, accessed June 16, 2023.

Table A.2: Herbicide Exposure and Contemporary Population Size, Naive OLS Estimates

	Panel A: ln Population (2001)				
	(1)	(2)	(3)	(4)	(5)
ln HERB	-0.059*	-0.050	-0.040	-0.046	-0.056*
	(0.034)	(0.030)	(0.028)	(0.028)	(0.029)
Adjusted R ²	0.716	0.793	0.815	0.819	0.822
	Panel B: ln Population (2020)				
	(1)	(2)	(3)	(4)	(5)
ln HERB	-0.075*	-0.070**	-0.058*	-0.068**	-0.082**
	(0.038)	(0.035)	(0.032)	(0.033)	(0.034)
Adjusted R ²	0.703	0.775	0.796	0.800	0.804
Observations	522	522	522	522	522
Avg. N neighbors (Conley SE cluster)	27.4	27.4	27.4	27.4	27.4
Key Target Covariates	✓	✓	✓	✓	✓
Geographic Covariates		✓	✓	✓	✓
Historical Covariates			✓	✓	✓
ln Spatially-Lagged HERB					✓
Fixed effects and $f(\text{Lon}, \text{Lat})$	✓	✓	✓	✓	✓

Notes: * $p < 0.1$; ** $p < 0.05$; *** $p < 0.01$. Conley (1999) standard errors adjusted for spatial clustering with a 30 km cutoff and a Bartlett kernel are in parentheses. Key target covariates: NVA base distance, population (1967–1969), U.S. base distance, U.S. troop distance, rice cropland, road distance, slash and burn cropland, Viet Cong control prevalence. Geographic covariates: Precipitation, wind speed, elevation, flow accumulation, forest presence, rice suitability, river distance, ruggedness. Historical covariates: Bombing point distance, border distance, number of neighbor hamlets, railway distance. ln spatially-lagged HERB is the logged average HERB among the neighbor hamlets with a 30 km cutoff. Fixed effects: Agent fixed effect, district fixed effect, end-edge fixed effect, pre-1967 mission fixed effect.

A.5 Naive OLS Estimates

Table A.2 reports the uninstrumented, naive ordinary least square (OLS) version of the main fuzzy regression kink (RK) specification with population size in 2001 and 2020 as outcomes. As briefly reported in the main text, compared with the main RK estimates, the naive OLS estimates underestimate or even fail to detect the negative association between herbicide exposure and contemporary population size revealed in Table 1.

The RK-OLS discrepancy may reflect (1) bias in the OLS estimates induced by confounding bias and measurement error, (2) bias in the RK estimates, (3) bias in both estimates, and (4) the difference in the estimands (average treatment effect, ATE, and the LAR or TT effect). Given the nonrandom nature of herbicide assignment, we mainly attribute the difference between the OLS and RK estimates to the bias remaining in the OLS estimates.

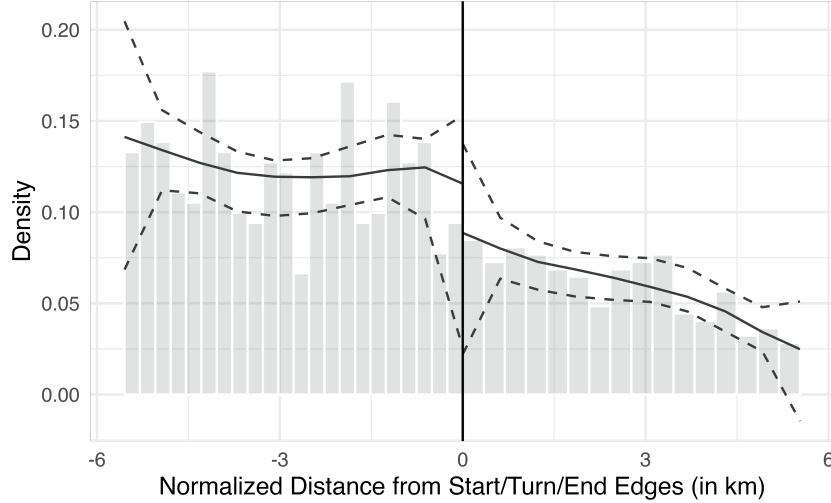


Figure B.1: Continuity of the Running Variable Distribution

Notes: Gray bars represent the histogram estimates of the running variable, EdgeDist. Solid and dashed lines indicate the local polynomial density estimates and the corresponding 95% confidence intervals (Discontinuity test: $t = -0.209$ and $p = 0.835$). The discontinuity estimate is computed using the procedure of Cattaneo, Jansson, and Ma (2020), with the running variable recentered at zero.

B Identification Assumption

B.1 Running Variable Distribution

A valid fuzzy RK design hinges on the smoothness assumption, which yields several testable implications (Card, Lee, Pei et al., 2015). The first testable implication of the smoothness assumption requires a running variable continuously differentiable at the kink point. To empirically validate the implication, Figure B.1 examines the continuity of the running variable using the estimator of Cattaneo, Jansson, and Ma (2020). Consistent with the identification assumption, the density test fails to detect discernible or statistically significant discontinuity in the running variable at the kink point ($t = -0.209$ and $p = 0.835$).

Second, the smoothness assumption requires not only the absence of discontinuity but also the absence of a slope change in the running variable distribution at the kink point. To further validate the assumption, we follow the approaches of Bana, Bedard, and Rossin-Slater (2020), Card, Johnston, Leung et al. (2015), Card, Lee, Pei et al. (2015), and Landais (2015) and test for the kink in the running variable distribution via polynomial regressions.

Formally, and with abuse of notation, we first aggregate the hamlet observations using bins with different sizes based on the running variable and then estimate the following regression model:

$$N_b^{\text{obs.}} = \beta \mathbb{1}[\overline{\text{EdgeDist}}_b \geq 0] + \sum_{p=1}^P \left[\gamma_p \overline{\text{EdgeDist}}_b^p + \delta_p \overline{\text{EdgeDist}}_b^p \cdot \mathbb{1}[\overline{\text{EdgeDist}}_b \geq 0] \right] + e_b, \quad (\text{B.1})$$

where b indexes bins, $N_b^{\text{obs.}}$ reflects the number of observations in each bin, $\overline{\text{EdgeDist}}$ is the midpoint of EdgeDist of each bin, and P is the polynomial order. The coefficient on the interaction between the linear of the running variable and the treatment group indicator, δ_1 , captures the change in the slope of the probability density function of the running variable at the kink point. We repeatedly estimate the polynomial regression using different bin widths ranging from 50 meters to 500 meters with an increment of 50 meters and the running variable polynomial orders ranging from 2 to 6.

Figure B.2 summarizes the polynomial regression results by plotting the coefficient estimates on the interaction term between the treatment group indicator and the (linear) running variable (δ_1). Triangles in each panel and Panel (f) indicate the estimates obtained from the smallest Akaike Information Criterion (AIC) value for each bin size. Regardless of the bin size and polynomial order, the coefficient estimates remain statistically insignificant at the 5% level. The polynomial regressions reveal no discernible slope change in the running variable distribution at the kink point and fail to invalidate the current RK strategy.

B.2 Covariate Distribution

Another key testable implication of the smoothness assumption involves covariate distributions around the kink point. The validity of the current RK design would be undermined if predetermined covariates, along the treatment, exhibit discernible kink around the cutoff.⁶

⁶Seen from the instrumental variable (IV) perspective, a key assumption here is that the instrument, $\text{EdgeDist} \times \mathbb{1}[\text{EdgeDist} \geq 0]$, affects the outcome (slope change) only through the treatment (slope change). A kink in a covariate can also be viewed as a sign of exclusion restriction violation such that the instrument affects the outcome through the covariate, not exclusively through the treatment.

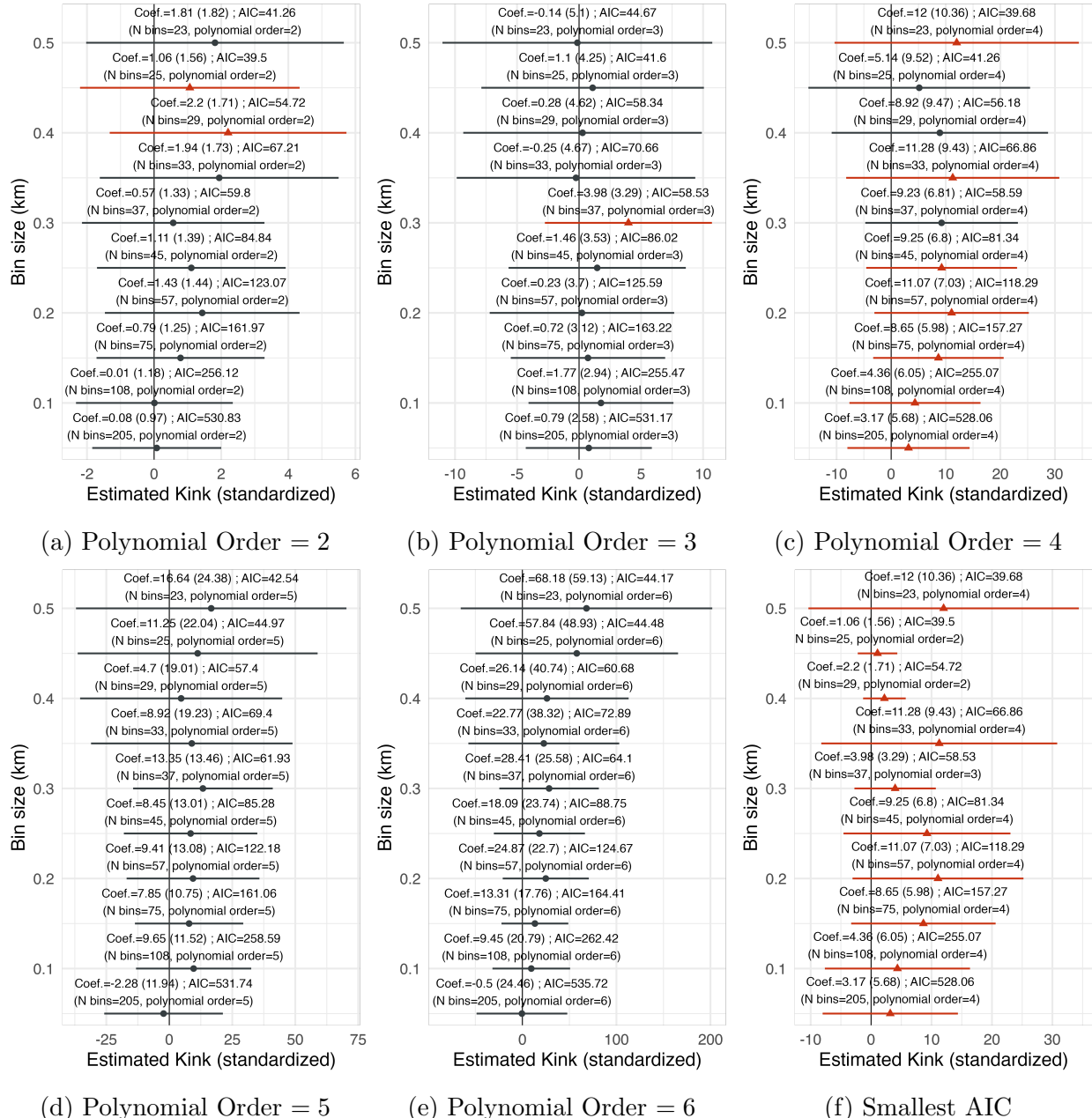


Figure B.2: Kink Estimates in the Running Variable Distribution

Notes: Dots represent the kink estimates obtained from polynomial regressions (δ_1 in equation B.1), with the running variable polynomial order specified as in the figure labels and bin sizes on the vertical axis. Triangles represent the estimates obtained from the model with the smallest Akaike Information Criterion (AIC) for each bin size. Horizontal segments represent the 95% confidence intervals.

We examine the validity of the assumption by subsequently estimating the first-stage specification of equation (2) with the left-hand-side variable, ln HERB, replaced by one of the covariates. We estimate the placebo kink estimate with and without adjustments for the re-

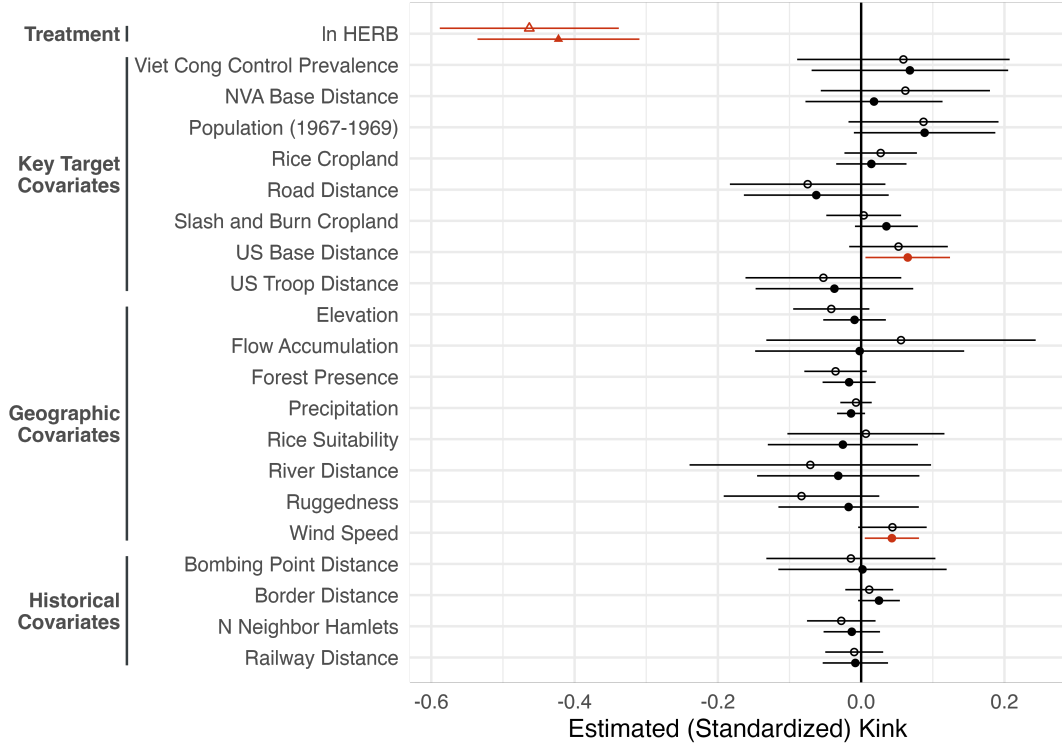


Figure B.3: (Standardized) Covariate and Treatment Kink Estimates

Notes: Symbols represent the reduced-form kink estimates with the variable on the vertical axis as the outcome variables, with (solid) and without adjustment for the remaining covariates (hollow). Horizontal segments represent 95% confidence intervals based on Conley (1999) standard errors with a 30 km cutoff and a Bartlett kernel (not corrected for multiple testing). All nonbinary variables are standardized.

maining covariates, with the baseline bandwidth $b = 4$ km as in Table 1 in the main text. The smoothness assumption requires that the coefficient on $\text{EdgeDist} \times \mathbb{1}[\text{EdgeDist} \geq 0]$ remains indistinguishable from zero once we replace the left-hand-side variable with covariates.

Figure B.3 summarizes the (standardized) kink estimates with (hollow symbols) and without adjustments for the remaining covariates (solid symbols), along with the treatment kink estimates (top row triangles). In a sharp contrast with the treatment slope change, and consistent with the identification assumption, most of the placebo regressions fails to detect a discernible slope change around the kink point. Exceptions include the substantively small but statistically significant estimates for wind speed (coef. = 0.043, $t = 2.299$) and U.S. base distance (coef. = 0.065, $t = 2.166$), along with the marginally significant estimates in population in 1967–1969 (coef. = 0.089, $t = 1.764$) and border distance (coef. = 0.025, $t =$

1.681), when adjusted for covariates (solid symbols).⁷

Nonetheless, the running variable (RV) randomization exercise disagrees with asymptotic inference and fails to negate that the covariate kink are generated by chance. As in Table 1, we randomly assign the running variable to the sample hamlets and estimate the placebo kink coefficient for 10,000 times. The randomization two-sided p -value indicates the share of the absolute placebo coefficients that are larger than the absolute actual coefficient. Figure B.4 shows the histograms of the placebo (standardized) kink estimates, with the corresponding actual kink estimates (vertical lines). The corresponding randomization p -values are 0.073 (wind speed), 0.068 (U.S. base distance), 0.101 (population, 1967–1969), and 0.147 (border distance) with covariate adjustments, and 0.095 (wind speed), 0.189 (U.S. base distance), 0.125 (population, 1967–1969), and 0.529 (border distance) without covariate adjustments.

A natural and substantively important question is on how the covariate kink affects the main RK estimates. A focused exercise in Appendix C, however, suggests that the RK estimates remain stable across all possible model specifications (covariate combinations) and outcomes, and reveals little sign of model dependence. Along with the little evidence of model dependence, the covariate kink test also fails to invalidate the current RK design.

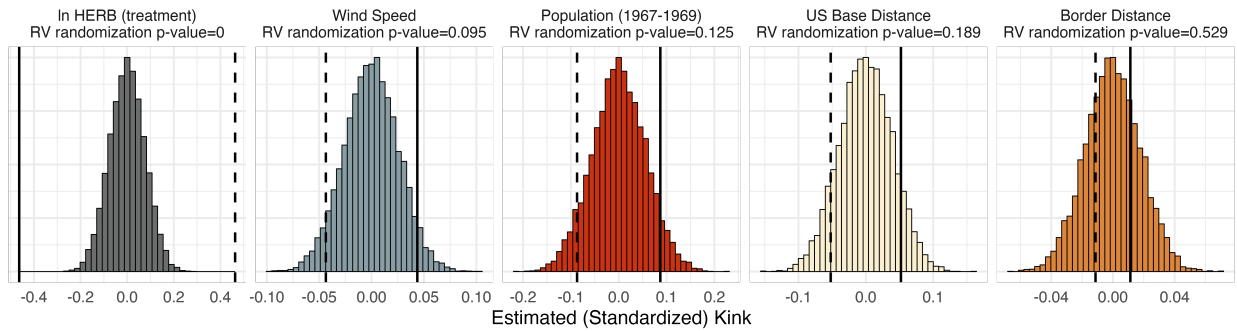
C Robustness Check

C.1 Confounding Nonlinearity and Model Dependence

One may wonder how the asymptotically significant kink in wind speed and U.S. base distance and model specification influence the main findings. Related to this point, Ando (2017) underlines the potential susceptibility of RK estimates to the failure to adjust for confounding nonlinearity. A simple, crude way to address this concern for confounding nonlinearity is to estimate all possible model specifications. The key idea is that if the current RK design

⁷Given one treatment and 20 covariates (21 variables) in Figure B.3, the probability of a Type I error in which one falsely rejects at least one null hypothesis with $\alpha = 0.05$ is 65.9% ($1 - 0.95^{21} = 0.659$).

Without Covariate Adjustment



With Covariate Adjustment

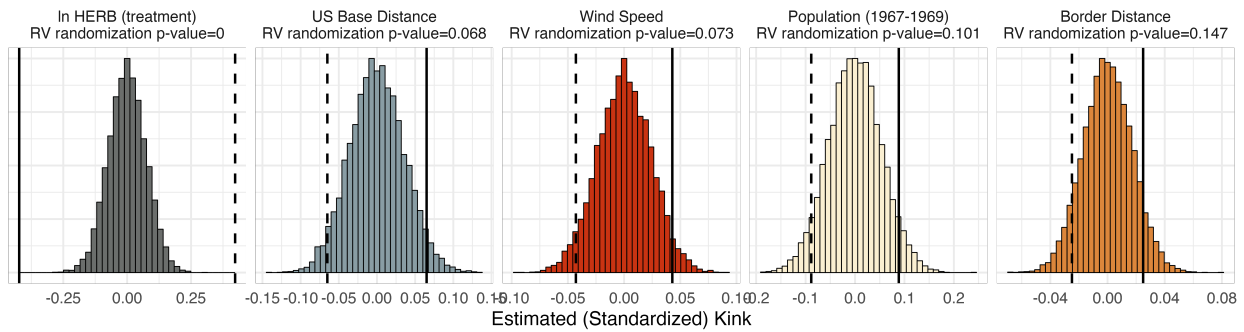


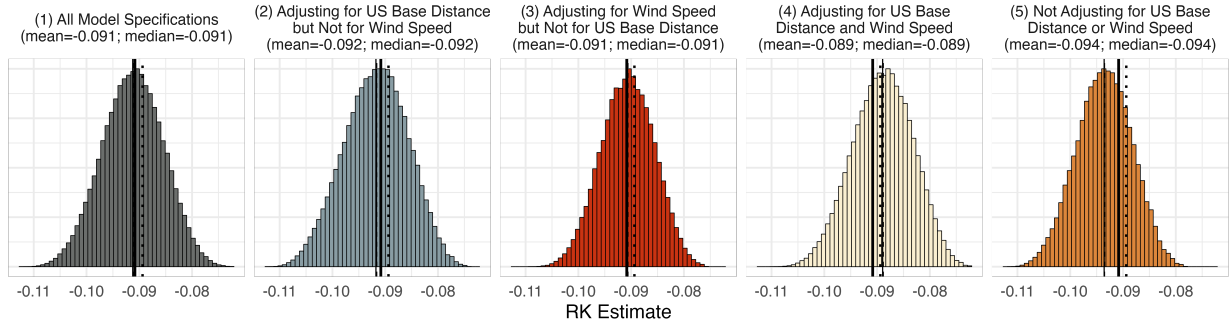
Figure B.4: Running Variable Randomization Inference

Notes: Each panel shows the histogram of 10,000 placebo kink estimates for the outcome in the top label. We randomly assign (permute) the running variable to the sample hamlets, and then estimate the reduced-form (or first-stage) version of the RK specification with (bottom row panels) and without covariate adjustments (top row panels) for 10,000 times. Solid (dashed) segments indicate the actual kink estimates ($-1 \times$ actual kink estimate) with the observed running variable. The randomization (two-sided) *p*-values in the top labels indicate the share of the absolute placebo coefficients that are larger than the absolute actual coefficient (vertical lines).

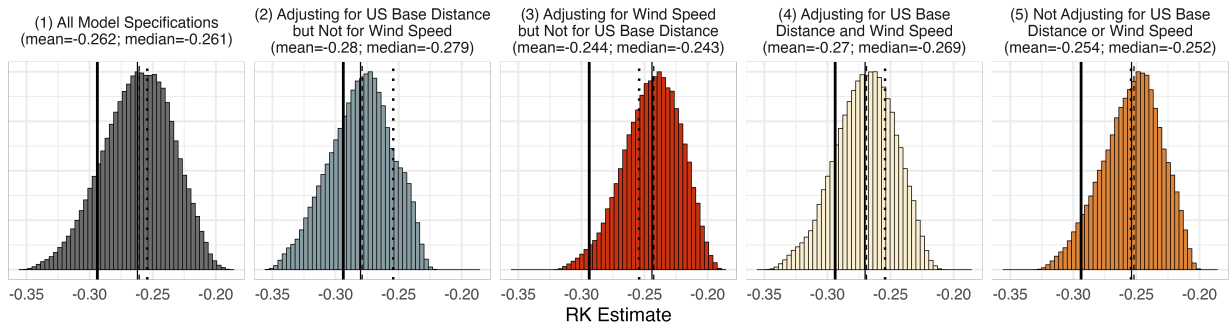
suffers confounding kink in observed outcomes, the RK estimate should be sensitive to the choice of covariate adjustments. Specifically, we repeatedly estimate the RK model with each covariate combination and three cross-sectional outcomes.⁸ Given that our RK specification includes 20 covariates along with the fixed effects and the longitude-latitude polynomial, the number of possible model specifications amounts to $2^{20} = 1,048,576$ for each outcome (omitting the spatially-lagged treatment and interaction terms). We estimate each model specification using the sample hamlet with the baseline bandwidth of $b = 4$ km as in Table 1 in the main text.

⁸This exercise relies on the cross-sectional setup given the qualitative similarity of annual (panel) and overall (cross-sectional) population growth rate estimates in Figure 4 in the main text.

Outcome: Overall Population Growth Rate (2001-2020)



Outcome: In Population (2020)



Outcome: In Population (2001)

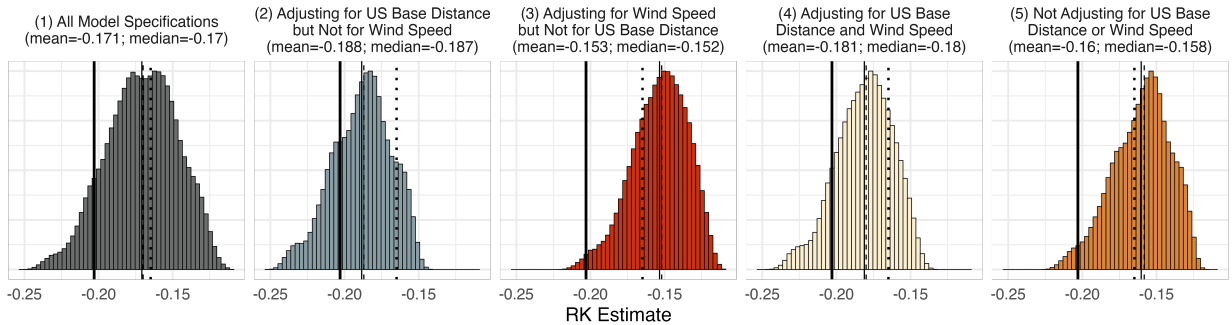


Figure C.1: Empirical Distribution of Second-Stage RK Estimates, All Possible Specifications

Notes: Density histograms in each row plot the empirical distributions of (subsets of) $2^{20} = 1,048,576$ RK model specifications for three cross-section outcomes, with different covariate adjustment conditions denoted in the top text labels. Thin solid and dashed vertical segments indicate the mean and median estimates in each panel. Bold solid and dotted vertical segments represent the RK estimates of model 1 (without covariates, solid) and model 4 (with all covariates, dotted) in Table 1 in the main text.

Figure C.1 summarizes the result of the “try-all” exercise. To explicitly examine how the adjustment for U.S. base distance and wind speed affect the estimates, Figure C.1 presents density histograms for RK estimates of, from the left, (1) all possible 1,048,576 models, (2) $2^{18} = 262,144$ models adjusting for U.S. base distance but not for wind speed, (3) 262,144 models adjusting for wind speed but not for U.S. base distance, (4) 262,144 models

adjusting for both U.S. base distance and wind speed, and (5) 262,144 models not adjusting for U.S. base distance or wind speed for each outcome. Thin solid and dashed vertical segments indicate the corresponding mean and median estimates, and bold solid and dotted segments indicate the RK estimates corresponding to Model 1 (without covariates) and Model 4 (adjusting for all covariates) in Table 1 in the main text.

The key results are threefold. First, across the outcomes, the empirical distribution of RK estimates is close to a normal distribution (with slight skews in population size in 2001 and 2020), suggesting that covariate combination does not play a major role in altering the RK estimates beyond random error. Second, the adjustment for U.S. base distance and wind speed is unlikely to alter the RK estimate. As graphically illustrated by the similarity between the panels in each row, the RK estimate distribution remains almost unchanged regardless of covariate adjustments, with almost identical sample mean (solid vertical segment) and median estimates (dashed segment). Third, the baseline RK estimates in Table 1 and Figure 4 in the main text (bold solid and dotted segments) are close to the means and medians of the empirical coefficient distributions (leftmost panels). Models with the full set of covariates (dotted segments) are almost identical to the mean and median estimates, and models without covariates (bold solid segments) slightly underestimate (population growth rate, Figure 4 in the main text) or overestimate (population in 2001 and 2020, Table 1 in the main text) while some of the covariates can be seen as posttreatment or a “bad control.” Combined, these results suggest that the covariate kink and the choice of covariate adjustments are unlikely to affect the inference severely, and the main findings are unlikely to be a product of arbitrary model picking or (observed) confounding nonlinearity.

C.2 Flight Buffer Width and Half-Decay Distance

Admittedly, the main RK estimates rely on an arbitrary combination of two parameters, flight buffer width and half-decay distance, to obtain the RK sample and measure the hamlet-level herbicide exposure score, HERB. As explained in Section 3 of the main text

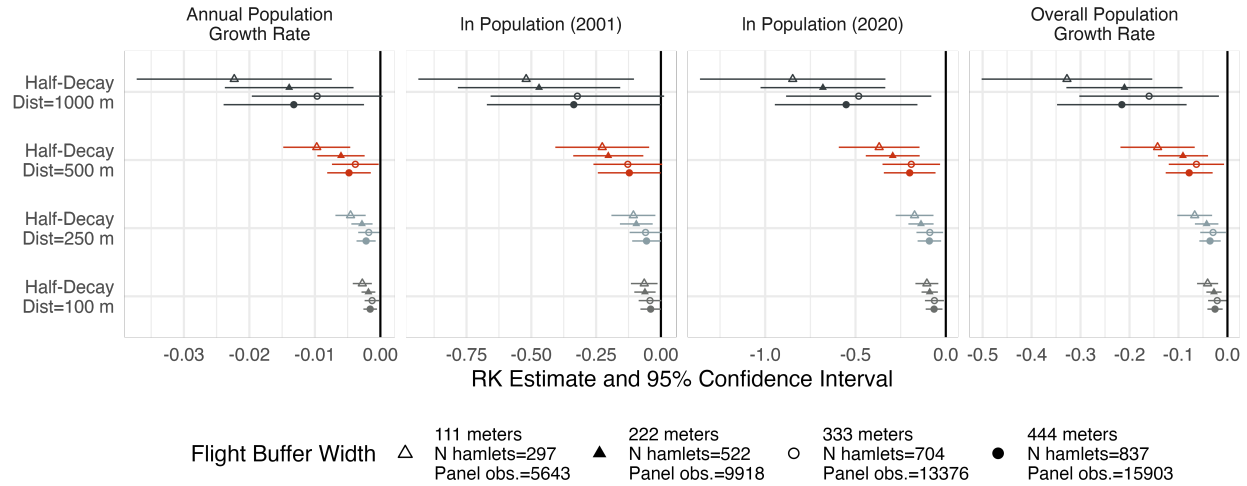


Figure C.2: RK Estimates with Different Flight Buffer Width and Half-Decay Distance Settings
Notes: Symbols represent the second-stage RK estimates with different flight buffer widths (indicated by symbols) and the half-decay distance parameter on the vertical axis, for each of the outcome variables in the column labels. Horizontal segments display the 95% confidence intervals based on Conley (1999) standard errors with a 30 km cutoff and a Bartlet kernel for the cross-sectional specification and hamlet-level clustering for the panel setup. Red solid triangles with half-decay distance = 500 m indicate the baseline estimates reported in Table 1 and Figure 4 in the main text. All estimates rely on the baseline bandwidth of 4 km and the model specification of model (1) in Table 1. Panel specification further adjusts for a year fixed effect.

and Section A.3, flight buffer width defines the sample hamlets used in the RK estimation, and the half-decay distance parameter determines HERB (eq. 1 in the main text).

To examine the robustness to the particular parameter setting, Figure C.2 reestimates the RK model with alternative parameter combinations. While the coefficient size varies, the negative association between herbicide exposure and contemporary population outcomes remains robust across different RK samples and distance-decay parameter values.

C.3 Counterinsurgency Strategy and Jackknife Estimates

A remaining but important concern for the current RK design is that the results might be driven by *unobserved* confounding kink such as counterinsurgency strategies and authorization procedure of herbicide missions. During the Vietnam War, the U.S. military divided South Vietnam into four Corps Tactical Zones (CTZs) commanded by different military branches and implemented distinct counterinsurgency strategies in individual CTZs. Dell

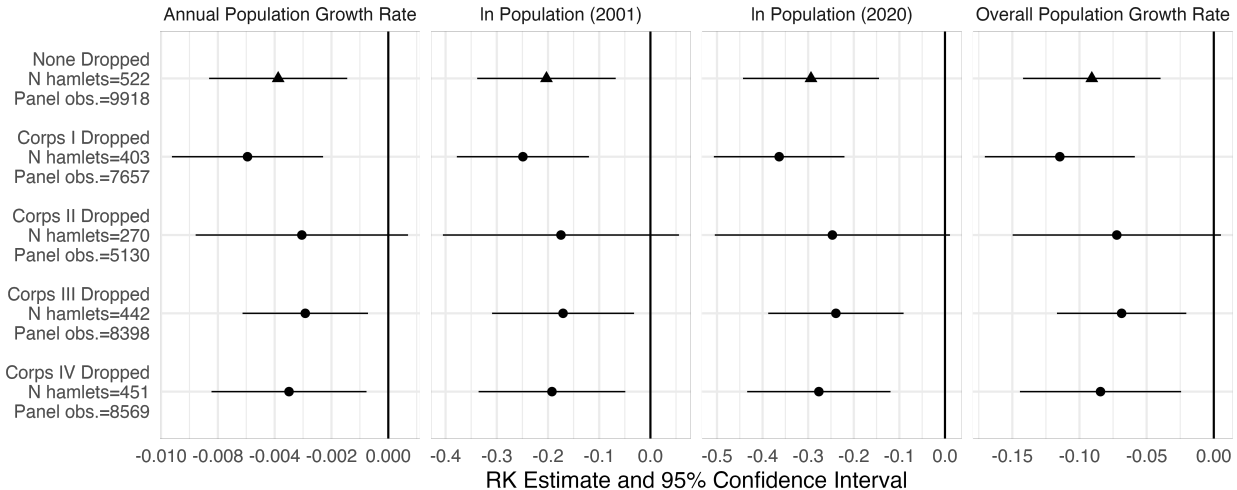


Figure C.3: Corps Tactical Zone-Level Jackknife

Notes: Symbols represent the RK estimates with subsamples dropping the hamlets in the Corps Tactical Zone on the vertical axis. Horizontal segments display the corresponding 95% confidence intervals based on standard errors with a 30 km cutoff and a Bartlet kernel for the cross-sectional specification and hamlet-level clustering for the panel setup. All estimates rely on the baseline bandwidth of 4 km and the specification of model (1) in Table 1. Panel specification further adjusts for a year fixed effect.

and Querubin (2018, 51–54) exploit the CTZ I–II boundary as one of the sources for causal identification, given the historical fact that the U.S. Marine Corps (USMC) in Corps Region I implemented a moderate hearts-and-minds-oriented strategy and small-unit operations, while the U.S. Army commanded Corps Region II and emphasized overwhelming firepower and large-scale operations. Similarly, as briefly explained in the main text, the authorization process of herbicide missions involved the South Vietnam Government, both at the national and local levels, and the U.S. at the levels of the U.S. Ambassador, the commander of the U.S. Military Assistance Command, Vietnam (MACV), and the CTZ commanders (Buckingham, 1982, 37; Institute of Medicine, 1995, 86).

Although the baseline specification includes a district fixed effect, we rely on CTZ-level and province-level jackknife approaches to more explicitly gauge the impact of the CTZs and corresponding differences in counterinsurgency strategies have on the reported RK estimates. Figure C.3 reports the jackknife estimates using a subsample dropping the hamlet observations located in the CTZ on the vertical axis. As the CTZ boundaries follow the

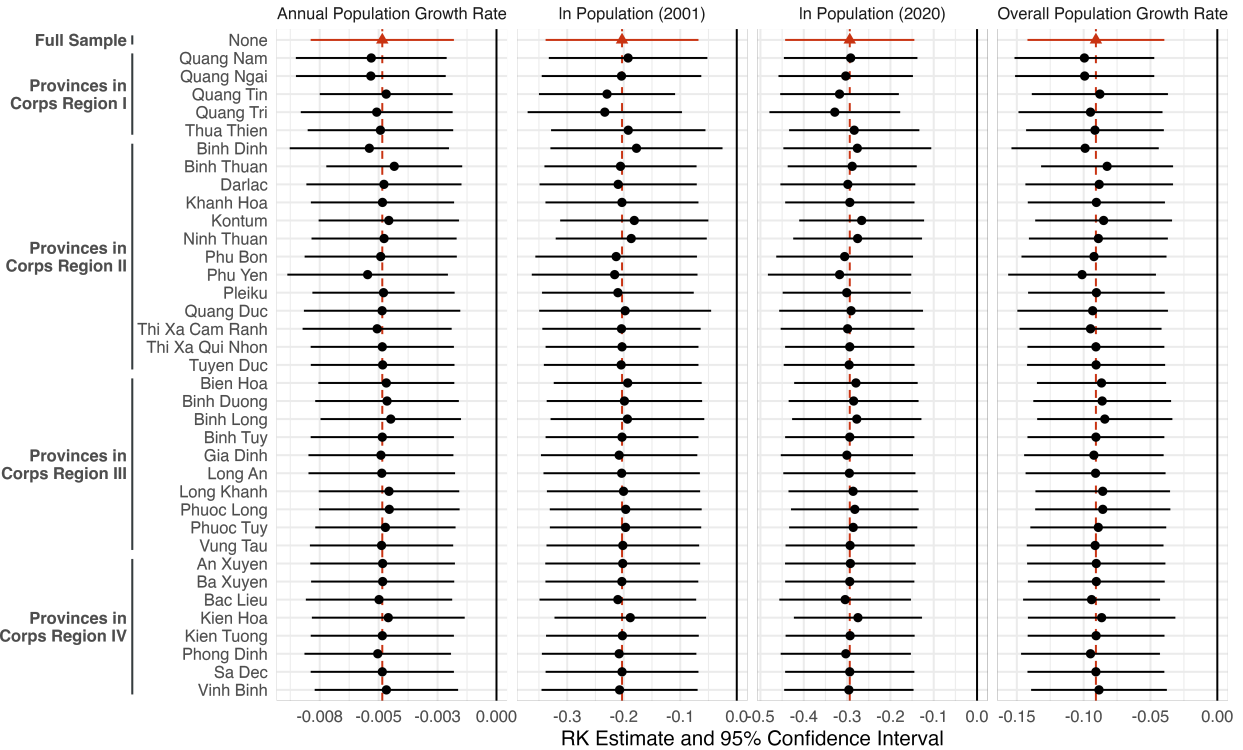


Figure C.4: Province-Level Jackknife

Notes: Symbols represent the RK estimates with subsamples dropping the hamlets in the province on the vertical axis. Horizontal segments display the corresponding 95% confidence intervals based on standard errors with a 30 km cutoff and a Bartlet kernel for the cross-sectional specification and hamlet-level clustering for the panel setup. Triangles and vertical dashed segments indicate the baseline estimate in Table 1 and Figure 4 in the main text. All estimates rely on the baseline bandwidth of 4 km and the model specification of model (1) in Table 1. Panel specification further adjusts for a year fixed effect.

preexisting provincial boundaries, and given the role of province chiefs in Ranch Hand missions, Figure C.4 presents a similar jackknife exercise in which hamlet observations in the province on the vertical axis dropped from the subsample for RK estimate. While the sample size and statistical significance vary, the negative coefficient estimates remain qualitatively unchanged across subsamples.

C.4 Unobserved Confounding Forces and Sensitivity Analysis

We also use a sensitivity analysis approach to examine how sensitive the main findings are to unobserved confounding nonlinearity. Table C.1 reports the reduced-form and first-stage versions of the main RK specification in Table 1 in the main text. The “robustness values” in

each panel indicate the percentage of residual variance that unobserved confounders would need to explain away the reported kink estimates (Cinelli and Hazlett, 2020). For both reduced-form and first-stage estimates, the robustness values suggest only implausibly strong unobserved confounders are capable of eliminating the main RK estimates.⁹ More precisely, the robustness values indicate that unobserved confounders would need to explain at least 16.59% (Model 4, Panel A) and 27.47% (Model 4, Panel B) of instrument ($\text{EdgeDist} \times \mathbb{1}[\text{EdgeDist} \geq 0]$) and left-hand-side variable (population 2020 in Panel A and $\ln \text{HERB}$ in Panel B) residual variance to eliminate the RK estimates in Table 1 in the main text. Given the battery of covariate adjustments in addition to the geocoordinate polynomial and fixed effects, it is implausible that a (combination of) confounding kink is driving the finding.

References

- Ando, Michihito. 2017. How much should we trust regression-kink-design estimates? *Empirical Economics* 53 (3):1287–1322.
- Bana, Sarah H., Kelly Bedard, and Maya Rossin-Slater. 2020. The Impacts of Paid Family Leave Benefits: Regression Kink Evidence from California Administrative Data. *Journal of Policy Analysis and Management* 39 (4):888–929.
- Buckingham, William A. 1982. *Operation Ranch Hand: The Air Force and Herbicides in Southeast Asia, 1961-1971*. Washington, DC: Office of Air Force History.
- Card, David, Andrew Johnston, Pauline Leung, Alexandre Mas, and Zhuan Pei. 2015. The effect of unemployment benefits on the duration of unemployment insurance receipt: New evidence from a regression kink design in Missouri, 2003-2013. *American Economic Review* 105 (5):126–130.
- Card, David, David S. Lee, Zhuan Pei, and Andrea Weber. 2015. Inference on Causal Effects in a Generalized Regression Kink Design. *Econometrica* 83 (6):2453–2483.
- Cattaneo, Matias D., Michael Jansson, and Xinwei Ma. 2020. Simple Local Polynomial Density Estimators. *Journal of the American Statistical Association* 115 (531):1449–1455.
- Cinelli, Carlos, and Chad Hazlett. 2020. Making sense of sensitivity: Extending omitted

⁹We report reduced-form and first-stage estimates as the robustness value measures the strength of unobserved confounding by partial R^2 . Note also that the RK estimand, τ_{RK} , can be written as the ratio of the reduced-form slope change (i.e., outcome slope change at the kink point) relative to the first-stage slope change (i.e., treatment slope change at the kink point) as (Card, Lee, Pei et al., 2015):

$$\tau_{\text{RK}} = \left(\frac{\lim_{v_0 \downarrow 0} d(\mathbb{E}[Y|V=v])}{dv} \Big|_{v=v_0} - \frac{\lim_{v_0 \uparrow 0} d(\mathbb{E}[Y|V=v])}{dv} \Big|_{v=v_0} \right) / \left(\frac{\lim_{v_0 \downarrow 0} d(\mathbb{E}[D|V=v])}{dv} \Big|_{v=v_0} - \frac{\lim_{v_0 \uparrow 0} d(\mathbb{E}[D|V=v])}{dv} \Big|_{v=v_0} \right),$$

where V denotes the running variable, v_0 the kink point, and D the treatment. The reduced-form (first-stage) robustness value can be interpreted as a sensitivity measurement for the numerator (denominator).

Table C.1: Reduced-Form and First-Stage Estimates with Robustness Values

	Panel A: ln Population (2020)				
	(1)	(2)	(3)	(4)	(5)
EdgeDist $\times \mathbb{1}[\text{EdgeDist} \geq 0]$	0.204*** (0.053)	0.174*** (0.048)	0.162*** (0.045)	0.161*** (0.045)	0.161*** (0.045)
Robustness Value	17.79%	17.02%	16.85%	16.84%	16.88%
Adjusted R ²	0.708	0.778	0.800	0.802	0.805
	Panel B: ln HERB				
	(1)	(2)	(3)	(4)	(5)
EdgeDist $\times \mathbb{1}[\text{EdgeDist} \geq 0]$	-0.693*** (0.095)	-0.660*** (0.089)	-0.629*** (0.087)	-0.633*** (0.086)	-0.632*** (0.084)
Robustness Value	30.75%	31.36%	30.99%	31.64%	32.25%
Adjusted R ²	0.620	0.652	0.663	0.666	0.677
Observations	522	522	522	522	522
Avg. N neighbors (Conley SE cluster size)	27.4	27.4	27.4	27.4	27.4
Key Target covariates		✓	✓	✓	✓
Geographic covariates			✓	✓	✓
Historical covariates				✓	✓
ln spatially-lagged HERB					✓
Fixed effects and $f(\text{Lon}, \text{Lat})$	✓	✓	✓	✓	✓

Notes: * $p < 0.1$; ** $p < 0.05$; *** $p < 0.01$. Conley (1999) standard errors adjusted for spatial clustering with a 30 km cutoff and a Bartlett kernel are in parentheses. Key target covariates: NVA base distance, population (1967–1969), U.S. base distance, U.S. troop distance, rice cropland, road distance, slash and burn cropland, Viet Cong control prevalence. Geographic covariates: Precipitation, wind speed, elevation, flow accumulation, forest presence, rice suitability, river distance, ruggedness. Historical covariates: Bombing point distance, border distance, number of neighbor hamlets, railway distance. ln spatially-lagged HERB is the logged average HERB among the neighbor hamlets with a 30 km cutoff. Fixed effects: Agent fixed effect, district fixed effect, end-edge fixed effect, pre-1967 mission fixed effect. Robustness values indicate the percentage of residual variance that unobserved confounders would need to explain in order to eliminate the reported kink coefficients.

- variable bias. *Journal of the Royal Statistical Society. Series B: Statistical Methodology* 82 (1):39–67.
- Conley, Timothy G. 1999. GMM estimation with cross sectional dependence. *Journal of Econometrics* 92 (1):1–45.
- Dell, Melissa, and Pablo Querubin. 2018. Nation Building Through Foreign Intervention: Evidence from Discontinuities in Military Strategies. *Quarterly Journal of Economics* 133 (2):701–764.
- Grizonnet, Manuel, Julien Michel, Victor Poughon, Jordi Inglada, Mickaël Savinaud, and Rémi Cresson. 2017. Orfeo ToolBox: Open source processing of remote sensing images. *Open Geospatial Data, Software and Standards* 2 (1):15.
- Institute of Medicine (Committee to Review the Health Effects in Vietnam Veterans of Exposure to Herbicides). 1995. *Veterans and Agent Orange: Health Effects of Herbicides Used in Vietnam*. Washington, D.C.: National Academy Press.
- Landais, Camille. 2015. Assessing the welfare effects of unemployment benefits using the regression kink design. *American Economic Journal: Economic Policy* 7 (4):243–278.
- Rowley, Ralph A. (Office of Air Force History). 1975. The Air Force in Southeast Asia:

- FAC Operations, 1965–1970. Office of Air Force History, May 1975, available at: <https://media.defense.gov/2011/Mar/24/2001330117/-1/-1/0/AFD-110324-008.pdf>.
- Stellman, Jeanne Mager, Steven D. Stellman, Richard Christian, Tracy Weber, and Carrie Tomasallo. 2003. The extent and patterns of usage of agent orange and other herbicides in Vietnam. *Nature* 422 (6933):681–687.
- Stellman, Jeanne Mager, Steven D. Stellman, Tracy Weber, Carrie Tomasallo, Andrew B. Stellman, and Richard Christian. 2003. A geographic information system for characterizing exposure to Agent Orange and other herbicides in Vietnam. *Environmental Health Perspectives* 111 (3):321–328.
- Tveite, Håvard. 2015. The QGIS Thin Greyscale Image to Skeleton Plugin. <http://plugins.qgis.org/plugins/ThinGreyscale/>.